Bioactive and Antimicrobial Layer-by-Layer Assembly on Titanium Surface

A THESIS
SUBMITTED TO THE FACULTY OF
UNIVERSITY OF MINNESOTA
BY

Jeevan Prasaad Govindharajulu

IN PARTIAL FULFILLMENT OF THE REQUIREMENTS
FOR THE DEGREE OF
MASTER OF SCIENCE

Dr. Mrinal Bhattacharya, Advisor
Dr. Conrado Aparicio, Co-Advisor

May 2013

Acknowledgements

I sincerely thank Dr. Mrinal Bhattacharya for giving me this opportunity to pursue this thesis work under his tutelage. I would also like to thank him for providing financial assistance for my research work. I would like to express my gratitude to Dr. Conrado Aparicio for the unwavering support and valuable suggestions he provided during my time here. I thank Dr. Bo Hu for being a part of my thesis committee member and for the kind of support he gave me.

I am thankful to Dr. Helmut Hirt and Dr. Sven-Ulrik Gorr for their guidance in anti-bacterial experiments.

This research work would not have been possible without the help of my lab mates Xi Chen and Dr. Yuping Li. I thank them for their constant assistance with my research.

Finally, I thank my family and friends for lavishly providing me their love and support.

Abstract

The main contemporary problems in the dental implant industry are 1) formation of biofilm around the implant – a condition known as peri-implantitis and 2) inadequate bone formation around the implant – lack of osseointegration. Therefore, developing an implant to overcome these problems is of significant interest to the dental community. Chitosan has been reported to have good biocompatibility and also anti-bacterial activity. An osseo-inductive recombinant biopolymer (P-HAP), derived from the protein statherin has been reported to induce bone formation. In this study, chitosan/P-HAP bi-layers were built on titanium surface using layer-by-layer (LbL) assembly technique by exploiting the strong opposite electrostatic charge of each polymer. The LbL modified surfaces were characterized by contact angle measurement, diffuse reflectance infrared fourier transform spectroscopy (DRIFTS), atomic force microscopy (AFM) and X-Ray photoelectron spectroscopy (XPS). The substantial difference in water contact angle between consecutive layers, the representative peaks in DRIFTS and XPS, and the changes in topography between surfaces with different number of bi-layers observed in AFM indicated the successful establishment of chitosan/P-HAP LbL assembly on titanim surface. The LbL modified surfaces showed increased amount of biominerlization in osteogenic media (OS) supplemented with $CaCl_2$, which is attributed to the well-established property of statherin. The amount of mineralization increased with the number of bi-layers. The mouse pre-osteoblastic cell line (MC3T3) adhered well, but a significant effect on cell differentiation was not observed on the LbL- modified surfaces. Osteoblast differentiation is a key step in bone formation. The discussion on the main causes for the lack of cell differentiation is provided. Notably, the LbL- modified surfaces showed significant anti-bacterial activity against gram positive *Streptococcus gordonii*.

Table of Contents

List of Tables

List of Figures

1. Literature Review

1.1 Dental Implants and Associated Problems

Orthopedic implants are the ones which can restore the patient's physical condition, and thereby improving their quality of life significantly. It is expected that the burgeoning population across the world, numbering seven billion today, will eventually have many patients requiring orthopedic implants. The orthopedic industry's worldwide revenues are estimated to reach US$ 40 billion by 2015 (1) and it is forecast that this sector will become the largest by far within the medical devices industry in purely monetary terms (2).

There are several types of implants, such as hip, knee, spine, cranio-maxillo-facial and dental implants. The generic, contemporary problems faced by orthopedic implants are [i] infection and [ii] lack of implant integration into the adjacent bone tissue. These are very pronounced in the dental implant industry and are primarily responsible for most failures (3,4). The dental implant industry contributes approximately 10% to the orthopedic market, which accounts for US$ 4 billion (1). Annually, about two million dental implants are being used in the world and this number is expected to grow considerably as the aging population increases (3,5). Although the success rate of dental implants is about 90% for 10-15 years (3,4), the 10% rate of failure in this a huge market will lead to an exorbitant loss. Hence, it is evident that there lies a huge opportunity in attempting to decrease the rate of failure in dental implants in order to make them more effective.

Infection refers to the formation of a bacterial biofilm around the surface of the implant, which eventually leads to inflammation. The diseases that are associated with this inflammation are termed peri-implant diseases; and are of two types: peri-implant

mucositis and peri-implantitis. The first is the inflammation of soft tissues surrounding the implant without any bone loss around it (3). The plaque (bacteria)-induced peri-implantitis is a serious condition where, in addition to the inflammation, there is rapid bone loss around the implant which can also be lethal (3) and can prevent the implant from integrating into the adjacent bone.

Osseointegration is a condition in which the implant is in intimate contact with the bone tissue without any interruption by fibrous tissue. The clinical success of the implant is associated with its integration into the peri-implant bone (bone which is around the implant) (4). After the implantation, the healing process (mechanical interlocking between the bone and implant) takes around three to six months (6). Surface properties of the implant exercise tremendous influence on the rate and quality of osseointegration (7,8). Significant research has been undertaken to increase the rate of osseointegration by modifying the implant surface (9,10,11).

1.2 Bioactive Coatings on Dental Implants

Commercially-pure titanium has been extensively used to make dental implants (4) because of its suitable mechanical properties (high tensile strength and elastic modulus), corrosion resistance, and biocompatibility (12). In spite of possessing such properties, titanium lacks the ability to rapidly osseointegrate as it only integrates with the bone passively (13), because of which, bone formation around the titanium implant takes long (around three to six months). Therefore, there have been several researches conducted to increase titanium's bio-activity (4,10,14,15,16,17,18,19).

Molecules such as, RGD (sequences of amino acids Arg-Lys-Asp) have been immobilized on the implant surface to attract the osteoblast cells using integrin receptors (4). Since the osteoblast cells are primarily responsible for bone formation, having an

increased number of these cells on the implant surface would increase the rate of osseointegration process. Poly-L-lysine (PLL) has been electrostatically coupled with the titanium oxide layer, which in turn aided in RGD attachment (20). In addition, researchers have tried to covalently couple the molecules which can promote osseointegration (16,17,18). However, these treatments involve complex chemical reactions which expectedly add to the existing implant's cost.

Calcium phosphate (CaP) coatings which are stoichiometrically close to Hydroxyapatite (HAP) are amongst the other elements used to improve osseointegration. These CaP coatings can serve as a scaffolding material or as template to facilitate bone formation (21). The rationale for developing CaP formation (similar to HAP) lies in CaP being the mineral phase of the bone and as a result, having osteoconductive property. Making the surface mimic the natural bone-like condition can induce the pre-osteoblast cells to attach, proliferate, and differentiate with enhanced response (22, 23, 24). The important step in bone formation is the differentiation of pre-osteoblast cells into mature osteoblast cells. When these cells differentiate, they will release various proteins to enable the formation of bone. Hence, if an implant facilitates the growth of the CaP mineral (such as, hydroxyapatite) on its surface, it will be a very promising aid for bone formation. Although the CaP coatings on the implant surface may increase the rate of osseointegration, there may also be the risk of bacterial colony-formation (25). This is due to the fact that the roughness accompanied by this coating may provide niches that can protect the bacteria from the host defense-mechanisms (3).

1.3 Statherin-inspired biopolymer

Statherin is a 43-residue protein present in human saliva which is responsible for the regulation of mineralization occurring on the apatite surface (enamel). This protein

attaches itself strongly to the hydroxyapatite (present in the enamel) (26). The SN15 peptide (DSpSpEEKFLRRIGRFG) of this protein is reported (27) to have the highest affinity for the CaP mineral - hydroxyapatite (HAP). It has been proved that the statherin fragments bind themselves to the HAP by electrostatic attraction. The negatively-charged N terminal region and the helical conformation are primarily responsible for HAP adsorption (27). The SN_A15 sequence (DDDEEKFLRRIGRFG), which has negatively-charged aspartic acid residues in place of phosphoserines present in sequence, have an affinity for HAP, which is comparable to that of SN15. So, this sequence can be used to induce calcium phosphate nucleation and eventually form HAP (28), which can aid in bone formation (29,30).

Elastin like recombinamers (ELRs) are a class of recombinant polypeptides which have identical properties (physical) to that of native elastin (31). Elastin is a protein in an extracellular matrix with elastic characteristics. This can respond to stimuli (like temperature and pH), which imparts biomimetic properties to ELRs. The ELRs remain disordered at temperatures below the inverse transition temperature (ITT), but at temperatures above this, the polymer chain folds into an ordered structure (32). This bio-mimicking property can be deployed for the controlled release of drugs (28). Apart from this, these polypeptides have remarkable biocompatibility (31). Given the advances made by techniques in genetic engineering, the design and production of these protein-based polymers have been on the rise (33,34). The SN_A15 and elastin sequences have been coupled to have a polymer with the ability to induce CaP mineralization and simultaneously have bio-mimetic property (33).

1.4 Anti-bacterial Coatings on Dental Implants

Titanium is highly susceptible to bacterial colonization (35), which will eventually lead to implant-failure. The bacterial colonization leads to biofilm formation on the titanium surface. The biofilm structure is believed to aid the bacteria to evade the host defense mechanism and antibiotics (8). Some of the bacteria which are responsible for implant failure are *Actinobacillus actinomycetemcomitans*, *Prevotella intermedia*, *and Porphyromonas. gingivalis* (36). These periopathogens eventually cause the bone loss around the implant. In a typical dental implant, the infected tooth is removed. The site is then, treated with systemic antibiotics in order to get rid of the bacteria. The treated site is allowed to heal for three to six months (3). After complete healing, a secondary surgery is done for placing a new implant. Considering the amount of time and cost associated with the implant procedure, the ideal solution for implantation seems to involve a removal of the infected tooth (and its root structure) and the placement of an implant which can prevent the formation of the bacterial colony (3). Hence, there is need to incorporate anti-microbial properties to the dental implant. This has led to efforts to develop antimicrobial coatings on the implant surface (3).

One simple approach has been to increase the hydrophillicity of the surface. This enables the formation of monolayers of water molecules, which can reduce the adhesion of bacteria onto the implant surface. There have been reports suggesting that hydrophilic surface can better adsorb serum proteins and promote the attachment and differentiation of bone-forming cells (4). Fluorine-modified surfaces have been proved to be lethal for pathogenic bacteria (37), but their ability to support osseointegration has not been proven.

Silver ions are known for their anti-bacterial activity, as they can bind themselves with the proteins present inside the bacteria and inhibit cellular activities (38). These ions

have been incorporated on titanium's surface and have proved to be effective against bacterial biofilm formation (39).

Antibiotics-releasing coatings have been tried over the years. The implants having such coatings, however are effective only in the short run, which implies that this approach cannot prevent peri-implantitis after several years have elapsed (3). Coatings that consist of Poly-L-Lactide (PLLA) having antibiotics proved to be efficient against *Staphylococcus aureus*, but its ability to induce bone formation remains unknown (40). Since hydroxyapatite can promote osseointegration better, antibiotic drugs are often incorporated with HAP (41,42,43) in order to enhance bone-forming ability and initiate anti-bacterial activity. However, these studies concentrate only on examining the anti-bacterial properties of the coatings and not their ability to aid osseointegration.

1.5 Chitosan as anti-bacterial agent

Chitosan, which is produced by the deacetylation of chitin (extracted primarily from shrimp and crab shells) (44) is a co-polymer of β-1,4 linked D-glucosamine and the *N*-Acetyl-D-glucosamine. It is known for its biocompatibility and anti-bacterial activity (45,46) over the years due to which, it is prominently applied in the biomedical field.

Chitosan, apart from being inexpensive and readily available in large quantities (5), displays anti-bacterial activity against many pathogens (5, 44,47,48). Chitosan's anti-bacterial activity remains unclear till today, but it is believed that the positively-charged amines in chitosan attract the negatively-charged bacterial cell wall, causing it to disturb the cell dynamics (5,44,49,50,51). The number of amino groups present in chitosan is believed to influence its ability to kill the bacteria (50). Another suggested mechanism is the formation of polyelectrolyte complexes as a result of the interaction between the chitosan and the bacterial cell wall (52,53), due to which, the nutrient permeation

ceases. The anti-bacterial mode of action is partially understood by Raafat et al. (44). In this report, it is hypothesized that chitosan's interaction with the bacterial cell wall leads to a leakage of cellular components without pore formation. It also affects the membrane-bound energy generation pathways, thereby, inducing stress on the bacteria. Chitosan treatment had caused a significant change in the expression of many genes in bacteria. These results indicate that the mode of action is complex and there cannot be a single pathway by which chitosan can kill the bacteria. Since chitosan's anti-bacterial activity is contact-dependent, the bacteria can grow away from the chitosan membrane (5). The amount of chitosan adsorbed to the cells is higher in the case of gram-negative bacteria compared to the gram-positive bacteria (49). Apart from being an anti-bacterial agent, chitosan is also reported to be an excellent material for growing osteoblast cells (11,14,54) because chitosan has structural characteristics similar to various glycosaminoglycans and hyaluronic acids (55).

1.6 Layer-by-Layer Assembly Technique

To functionalize the titanium surface, one of the commonly used methods is the covalent bonding with bio-active molecules. As mentioned earlier, this may involve complex chemical reactions and consequently increase the implant costs. If the number of bio-active groups is high, it may enhance the activity of the attached molecule and sustain this for a longer period of time. It is clear that there are two properties which should be incorporated into the titanium surface: anti-bacterial and osseointegration. Two molecules should be used for this. Simply mixing the two molecules and coating the mixture onto the surface will not offer a uniform coating, so, it is imperative to exercise better control over the coating process. In order to use a simple, controllable technique, and yet have many functional groups on the surface, one can undertake the Layer-by-

Layer (LbL) Assembly. In addition, this technique can be used to anchor different molecules to the surface. Through the use of the electrostatic attraction between oppositely charged polyelectrolyte (PE) solutions, the technique enables the formation of nano scale layers on the surface. This is done by successively treating a surface with oppositely charged solutions (56). In this technique, the surface is initially treated so that a charge is imparted to it (say negative), after which it is treated in a solution having positively-charged molecules. The molecules attract each other electrostatically to form a layer. After this step, all unbounded or weakly bound molecules are washed and removed. This modified surface is again introduced into a negatively-charged solution to form a bi-layer and the process of alternate treatment is continued so that the desired number of bi-layers can be built. There are two main ways in which Layer-by-Layer Assembly can be accomplished namely, spin and dip assisted Layer-by-Layer technique. In the spin-assisted method, the PE solution is placed in the centre of the surface (oppositely-charged to the PE solution) to be coated and spun (using spin-coating equipment). To wash the surface, one can use either water or other solvents in place of the PE solution. In the dip-coating method, the surface is just immersed successively in one PE solution, water (or other solvent), and then, in another PE solution. In both the methods (spin and dip), the electrostatic attraction will lead to the formation of bi-layers. Although the spin coating takes comparatively less time than dip coating (57), the use of coating equipment can be avoided when one resorts to the dip method. The concentration of the PE solution is critical to getting layers with uniform thickness. If the concentration is very high (above 5 mg/ml), there will be increased thickness. On the other hand, if the concentration is low (below 0.1 mg/ml), then, the thickness will be quite low too. So, the ideal concentration of the polyelectrolyte solution would be around 0.1 to 5 mg/ml (58). Although the adsorption process gets completed in

a few minutes, the ideal time is about 20-30 minutes. The film thickness will be the same when all the parameters such as, concentration and pH are uniformly maintained. So, film thickness can be controlled to a great extent in the Layer-by-Layer technique. Apart from achieving uniform film thickness, this technique is attractive because of the versatility and simplicity with which the surface is functionalized (56, 59, 60). The only requirement of this technique is that the molecules to be coated should be oppositely-charged. Chitosan has been incorporated into the titanium surface using the LbL technique (14,15) and it has also been shown that it retained its anti-bacterial property even when coated by this technique (8,10, 60).

An ELP, named P-HAP whose amino acid sequence $[(VPGIG)_2$ $(VPGKG)$ $(VPGIG)_2]_2$ DDDEEKFLRRIGRFG $[(VPGIG)_2$ $(VPGKG)$ $(VPGIG)_2]_2$ has been successfully coated with chitosan on a glass surface using the LbL method (33) due to the fact that P-HAP is highly negatively charged and chitosan is positively charged. The activity of this composition has not been tested. Here, the bioactive region is DDDEEKFLRRIGRFG, which is the SN_A15 region described earlier and the repeating units of VPGIG are deemed responsible for the elastin property.

2. Hypothesis and Aim

This project aims to build P-HAP/Chitosan coatings on commercially pure titanium surface using the LbL assembly technique. The positively-charged chitosan (at acidic pH) and the highly negatively-charged P-HAP can effectively form bi-layers due to electrostatic attraction. The hypothesis of this work were: [i] the chitosan present in the LbL assembly will be an effective anti-bacterial agent to minimize the biofilm formation on the titanium implant surface [ii] The P-HAP present in the LbL assembly will enhance the differentiation of the osteoblast cells due its ability to form calcium phosphate minerals. Consequently, this new coating will be effective in terms of favoring rapid osseointegration, as well as rendering anti-bacterial activity.

3. Materials and Methods

3.1 Materials

All the chemicals have been purchased from Sigma – Aldrich (Saint Louis, MO) unless indicated specifically. Mouse pre-osteoblastic cell line MC3T3-E1 subclone 15 was provided by Dr. Eric Jensen, School of Dentistry, University of Minnesota – Twin Cities. *Streptococcus gordonii* (ML-5) strain was provided by Dr. Helmut Hirt, Diagnostic and Biological Sciences, University of Minnesota – Twin Cities. Statherin derived bio-polymer (denoted as P-HAP) having amino acid sequence $[(VPGIG)_2$ (VPGKG) $(VPGIG)_2]_2$ DDDEEKFLRRIGRFG $[(VPGIG)_2$ (VPGKG) $(VPGIG)_2]_2$ was obtained from Professor Carlos Rodriguez-Cabello from the University of Valladolid, Spain as part of his collaboration with Professor Conrado Aparicio. Details of the fabrication of this polymer can be found in the literature (33,61,62, 63). Titanium discs (6mm diameter) were cut from commercially pure titanium grade II (McMaster Carr, Elmhurst, IL).

3.2 Sample preparation

The commercially pure (c.p) titanium discs were polished using 240 and 600 grit silicon carbide discs (Buehler, Lake Bluff, IL) for five minutes. This was followed by further polishing using 1μm and 0.5μm alumina suspension (Buehler, Lake Bluff, IL) for 1 hr. The polished samples were soaked overnight in acetone solution and washed with de-ionized water. The discs were then, ultra-sonicated in cyclohexane (BDH Chemicals, West Chester, PA) solution for 15 minutes, washed thoroughly with acetone and de-ionized water. After this, the discs were dried using nitrogen flow.

3.3 Fabrication of Layer-by-Layer Assembly

The chitosan solution (1 mg/ml) was prepared by dissolving chitosan (coarsely ground flakes and powder, deacetylation ≥ 75%, Molecular weight - >310,000 g/mol) in 2% (v/v) acetic acid solution (Ricca Chemical Company, Arlington, TX). The P-HAP (Molecular weight – 32 kDa) solution (0.5 mg/ml) was prepared in cold water (4^0C). The pH of both the solutions was adjusted to 4.5 using hydrochloric acid and sodium hydroxide (Macron Chemicals, Center Valley, PA). At this pH, the chitosan was positively-charged, whereas the biopolymer and titanium dioxide were negatively-charged.

The polished c.p Ti discs were cleaned using O_2-Plasma Cleaner PDC-32G (Harrick Plasma, Ithaca, NY) for 5 minutes. The plasma-treated c.p Ti discs (pTi) were immersed in chitosan solution for 30 minutes. The samples were then, rinsed using de-ionized water (pH 4.5), and dried. After complete drying, the samples were immersed in P-HAP solution for 30 minutes, rinsed using de-ionized water, and dried. This cycle was repeated to get the desired number of bi-layers. The LbL assembly process has been described in Figure 1. The nomenclature used to denote the appropriate treatments islisted in Table 1 below :

Table 1: Details of the nomenclature used for different treatments

Treatment	Name	No. of Chitosan layer(s)	No. of P-HAP layer(s)	Top layer
Plasma-treated titanium	pTi	0	0	TiO_2
Chitosan coated plasma-treated titanium	Ti+C	1	0	Chitosan
P-HAP coated plasma-treated titanium	Ti+P	0	1	P-HAP
One bi-layer on titanium	$(C+P)_1$	1	1	P-HAP
Ten bi-layers on titanium	$(C+P)_{10}$	10	10	P-HAP
Ten bi-layers with one additional chitosan layer	$(C+P)_{10}C$	11	10	Chitosan
Twenty bi-layers on titanium	$(C+P)_{20}$	20	20	P-HAP
Twenty bi-layers with one additional chitosan layer	$(C+P)_{20}C$	21	20	Chitosan

A

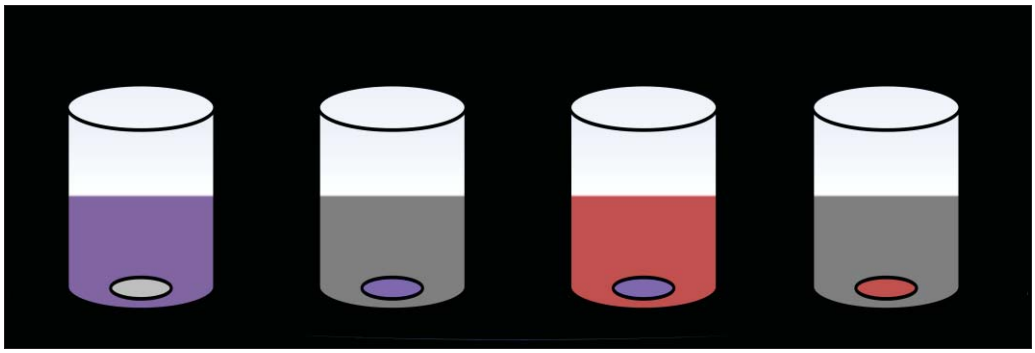

B

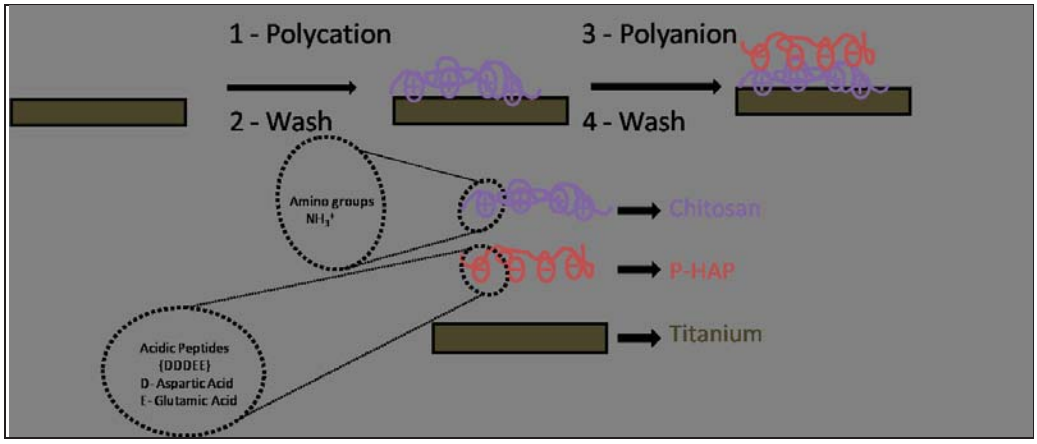

Figure 1: LbL Assembly Process. (A) Schematic of the LbL assembly process on titanium disc. Initially, the plasma treated disc is immersed in chitosan solution (step1) and then washed with water (step 2). The disc is then immersed in P-HAP solution (step 3) and washed with water (step 4). (B) Simplified molecular depiction of the first two adsorption steps. The polycation used here is chitosan and the polyanion is P-HAP.

3.4 Characterization of Layer-by-Layer Assembly

3.4.1 Contact angle measurement

The contact angle for pure titanium and after each layer build up was measured with water to have an understanding about the change in hydrophobicity / hydrophillicity nature during the LbL assembly. This measurement was performed using the sessile drop method (using 3 µl of de-ionized water). The drop was equilibrated on the surface for 30 seconds and the contact angle measurement was recorded for every second using a DM-CE 1 Contact Angle Meter (Kyowa Interface Science, Saitama, Japan). Since, it took approximately 25 seconds for the droplet to stabilize; the last four measurements (values of 27^{th} – 30^{th} seconds) were averaged for each sample. Three samples were used per treatment.

3.4.2 Diffuse Reflectance Fourier-transform infrared spectroscopy (DRIFTS)

The LbL-modified surfaces were analyzed using the Nicolet Series II Magna-IR System 750 FTIR in Diffuse Reflectance fourier-transform infrared spectroscopy (Nicolet Instruments, Madison, WI) to determine the characteristic peaks of chitosan and P-HAP. The wavenumber range scanned was from 648 to 4000 cm^{-1}. Plasma-treated Ti discs were used as control backgrounds to ascertain the characteristic peaks of the LbL-modified surfaces.

3.4.3 Atomic Force Microscopy (AFM)

The AFM characterization was done using a Dimension 3000 AFM (Digital Instruments, Santa Barbara, CA) in tapping mode at room temperature to monitor the

topography of the LbL-modified surfaces. The scan size was 3μm×3μm with a scan rate of 1Hz and with image resolution of 512 samples / line. The proportional and integral gains were set to 0.6 and 1.2 respectively with amplitude set points of 1.772V. The Average Roughness (R_a) and Surface Area Difference (S.A.D in %) were determined for each image.

R_a is the arithmetic mean of the surface height relative to the central plane. S.A.D is the measure of increase in surface area due to roughness which can be defined by the following equation (64):

$$\mathrm{S.A.D} = \left\{ \frac{\sum_{i=1}^{n} (Surface\ Area)_i}{\sum_{i=1}^{n} (Projected\ Area)_i} - 1 \right\} \times 100$$, where "n" is the number of points in the sample area.

Two-dimensional and three-dimensional images were taken to better understand the surface topography. Four different areas were scanned for each sample.

3.4.4 X-Ray Photoelectron Microscopy (XPS)

In order to analyze the chemical composition of the LbL-modified surfaces, XPS (SSX-100, Surface Science Instruments, Mountain View, CA) with focused monochromatic Al Kα X ray source was used. The electron take-off angle was 35^0 with spot size of 800μm. The scan range was from 0 to 1100 eV. One sample per treatment was analyzed.

3.5 Biomineralization

The multilayered samples were placed in 48 well plate (Costar, Corning, NY) and incubated in 1 ml of MEM-α medium (Invitrogen, Grand Island, NY), supplemented with 20mM $CaCl_2.2H_2O$, 10mM β-glycerophosphate, 50μg/ml ascorbic acid, 10% HyClone™

fetal bovine serum (Thermo Scientific, South Logan, Utah), and 1% penicillin-streptomycin (Invitrogen, Grand Island, NY) at 37^{o}C for 7 days. The medium was replaced every three days. Following the incubation period, the samples were dehydrated using increasing concentrations of ethanol from 60% to 100%. Plasma-cleaned samples were used as controls for this experiment.

3.6 Characterization of Biominerlization

3.6.1 Diffuse Reflectance Fourier-transform infrared spectroscopy (DRIFTS)

The biomineralized samples were analyzed using DRIFTS as previously described to find the characteristic peaks of phosphate. Plasma-treated Ti discs were used as the background.

3.6.2 Scanning Electron Microscope (SEM)

The samples were viewed under the tabletop Scanning Electron Microscope (TM 3000 – Hitachi, Tokyo, Japan) to visualize calcium phosphate mineral deposition on the multilayered samples. Images were taken at 10,000X and 20,000X for each sample. The images were obtained as combinations of the collated secondary and back-scattered electrons and thus, the images carried topographical and elemental / chemical information.

3.6.3 Energy Dispersive X-ray Spectroscopy (EDS)

To analyze the Calcium to phosphorus (Ca/P) ratio, we used an EDS microprobe with Quantax 70 software (Bruker, Fitchburg, WI) attached to the SEM equipment. Three different areas were analyzed per sample.

3.7 Osteoblast Cell culture

The mouse pre-osteoblast cell line (MC3T3-E1) was maintained in complete culture medium consisting MEM-α (Invitrogen, Grand Island, NY) supplemented with 10% fetal bovine serum (Gemini Bioproducts, Sacramento, CA) and 1% Penicillin-Streptomycin under standard cell culture conditions (37^0C in a humidified atmosphere of 5% CO_2). Cells were passaged (sub-cultured) every 3-4 days. For passaging, the cells were detached using 2 ml trypsin solution (0.075% trypsin in Hank's Balance Salt Solution (Invitrogen, Grand Island, NY)) from a petri-dish. The complete medium was added in excess to the detached cells and centrifuged at 1,500 rpm for 3 minutes. The cell pellet was re-suspended in complete medium and transferred into new petri-dishes.

3.8 Cell adhesion experiment

For the adhesion experiment, the treated titanium discs (n=3) were placed in 12 well plate (Costar, Corning, NY) and incubated in 70% ethanol under UV for 30 minutes. Wells without titanium discs, which are Tissue Culture Polystyrene (TCPS) served as positive controls. After incubation, ethanol was removed and the wells were washed thrice with Hank's Balance Salt Solution (HBSS). 200 µl of 5% Bovine serum Albumin (Thermo Scientific, South Logan, Utah) were seeded onto the samples (including control) and incubated for 30 minutes under UV to block any non-specific cell adhesion. The processed samples were transferred to fresh 48 well plate (Costar, Corning, NY). Pre-osteoblast cells were diluted using serum-free media (complete media without FBS) and seeded at a density of 2000 cells / well. The cells were allowed to be attached to the samples by incubating them at 37^0C in a humidified atmosphere of 5% CO_2 for 4 hrs.

After incubation, the cells were fixed using 4% paraformaldehyde (Fisher Scientific, Fair Lawn, NJ) for 20 minutes. The fixed cells were lysed by incubating in the

lysis buffer (1X Phosphate Buffered Saline (Invitrogen, Grand Island, NY), 0.3% Triton X-100 (Fisher Scientific, Fair Lawn, NJ)) for 5 minutes.

100 µl of Immunofluorescence (IF) solution (prepared by dissolving 1.5g Bovine Serum Albumin (Thermo Scientific, South Logan, Utah), 5 ml 10X Phosphate Buffered Saline (Invitrogen, Grand Island, NY), 0.5 ml 2M $MgCl_2$, and 150 Tween 20 (Fisher Scientific, Fair Lawn, NJ) in 50 ml double distilled H_2O) was added to the sample containing wells and incubated for 30 minutes to block non-specific binding.

The cells were stained for vinculin (using vinculin antibody), F-actin (using phalloidin), and nucleus (using DAPI). Vinculin was used to visualize focal contacts. Phalloidin (conjugated with rhodamine) bound to F-actin and stained it (65). 4',6-Diamidino-2-Phenylindole, Dihydrochloride (DAPI) stained the A-T regions of the DNA (66), as a result of which, the nucleus could be visualized. While Vinculin and F-actin staining offered information about cell spreading and number, and distribution of focal adhesion points, nucleus staining offered the number of cells adhered onto the sample.

The cells were stained for Vinculin by adding 30 µl of monoclonal anti-vinculin 1:500 diluted with IF solution on each of the samples and incubated at 37^oC for 4 hrs. This antibody will bind to the vinculin protein at focal adhesion points. Following incubation, the samples were washed thrice for 5 minutes with 300 µl washing solution having 1XPBS, 0.1% Triton X-100.

Alexa Fluor 488 goat anti-mouse IgG (H+L) (Invitrogen, Eugene, Oregon){secondary antibody which binds to anti-vinculin} diluted 1:600 in IF solution, DAPI (Invitrogen, Eugene, Oregon) diluted 1:1500, and rhodamine phalloidin (Invitrogen, Eugene, Oregon) diluted 1:5000 were mixed in 1.5 ml microcentrifuge tube. 30 µl of this mixture was added to the samples and incubated for 1 hr in the dark at 37^0C. Finally, the samples were washed thrice (1XPBS, 0.1% Triton X-100) and viewed under a Nikon

Eclipse E800 fluorescent microscope (Nikon, Melville, NY). Pictures were taken from three different areas per sample and the cells were counted using ImageJ 1.45 (NIH, Bethesda, MD).

3.9 Osteoblast Differentiation

To analyze osteoblast differentiation, the pre-osteoblast cells were seeded at the density of 20,000 cells/well on to the 48 well plate having samples (n=3). Calculations were made such that each well had 800 µl cell culture. Initially, complete medium was used and after confluence (3 days after seeding), the media was changed to differentiation media. The differentiation media comprised MEM-α medium (Invitrogen, Grand Island, NY), supplemented with 10mM β-glycerophosphate, 50µg/ml ascorbic acid, 10% HyClone™ fetal bovine serum (Thermo Scientific, South Logan, Utah), and 1% penicillin-streptomycin (Invitrogen, Grand Island, NY). Standard cell culture conditions (37^0C in a humidified atmosphere of 5% CO_2) were maintained. The media was changed every 3 days. Discs and the supernatant solution were taken after 7, 14, and 21 days of incubation. The supernatants were stored at -20^0C until used. The discs were used to quantify alkaline phosphatase activity and the total protein content, whereas the cell culture supernatant solution was used to quantify osteocalcin.

3.9.1 Cell lysate preparation

The discs (while in the plates) were washed with 1X PBS to remove any media. The cells were lysed using 300 µl lysis buffer {1% triton X-100, 0.1mM $MgCl_2$, 150 mM tris (Promega, Madison, WI) pH 10.5} for 10 minutes. Then, the cells were manually scrapped from the discs into buffer using a pipette tip. The scrapped cells along with the

lysis buffer were then transferred into 1.5 ml microcentrifuge tubes and then, centrifuged at 3000 rpm for 10 minutes at 4^{o}C. The supernatant was collected without disturbing the pellet and stored at -20^{0}C for alkaline phosphatase activity and total protein quantification.

3.9.2 Alkaline phosphatase activity quantification

Alkaline phosphatase (ALP) is an early differentiation marker for osteoblast cells. This assay measured the ALP activity based on the rate of conversion of p-nitrophenyl phosphate in the presence of 2-amino-2-methyl-1-propanol by ALP. The resulting p-nitrophenol could be measured at 410nm, which was directly proportional to the ALP activity in the sample.

Briefly, the procedure involved mixing 5 µl of the cell lysate solution with 100 µl of freshly prepared AMP reaction buffer (22.5 µl of 1:4 diluted 2-amino-2-methyl-1-propanol (Fluka, Switzerland), 12 µl $MgCl_2$, 2X 20 mg 4-nitrophenyl phosphate disodium salt hexahydrate tablets dissolved in 10 ml ddH_2O) in each well of the 96 well plate. This mixture was incubated for 2 hrs at 37^{0}C and the reaction was stopped by adding 25 µl of 2M NaOH solution to each well. The absorbance was read at 410nm using Beckman Coulter AD-340 spectrophotometer (Beckman Coulter, Fullerton, CA).

3.9.3 Total protein quantification

The total protein content in the cell lysate was measured in order to normalize the protein differentiation markers with the cell number. Bio-Rad *DC* protein assay kit was used to estimate the total protein content. This kit is based on the Lowry assay to quantify protein. In this assay, the copper in the alkaline medium reacts with protein.

This copper-treated protein reduces Folin reagent and imparts a blue color which has maximum absorbance at 405 - 750nm. The assay was performed according to manufacturer's instructions (*DC* Protein Assay Instruction Manual, Bio-Rad, Hercules, CA).

Briefly, the procedure involved the preparation of protein standards (0.2, 0.4, 0.6, 0.8, 1.0 and 1.2 mg/ml) by diluting bovine serum albumin in lysis buffer. 5 µl of cell lysate solution and protein standards were pipetted into 96 well plate (Costar, Corning, NY) and mixed with 25 µl of A' (prepared by mixing 1 ml reagent A and 20 µl reagent S). To this mixture, was added 200 µl of reagent B which was mixed and incubated for 15 minutes. Following incubation, the absorbance was read at 650nm using Beckman Coulter AD-340 spectrophotometer (Beckman Coulter, Fullerton, CA). Concentrations of the protein were calculated based on the standard plot.

3.9.4 Osteocalcin quantification in supernatant culture medium

Osteocalcin is a late differentiation marker for osteoblast cells which is present in the extra-cellular matrix. The osteocalcin protein quantification was performed using the Mouse Osteocalcin EIA kit (BT-470, Biomedical Technologies, Stoughton, MA). This kit is based upon sandwich Enzyme Immunosorbent Assay (EIA). A polyclonal antibody which is directed against N-terminus of osteocalcin is attached to polystyrene wells. Incubation with the sample (culture supernatant) would result in the binding of N-terminus of osteocalcin (in the sample) with the antibody coated to the well. A secondary antibody (biotinylated) specific for C-terminus of osteocalcin was then, used to sandwich the protein present in the sample. The biotinylated antibody (attached to osteocalcin) was detected by incubating with peroxidase-streptavidin conjugate and appropriate

substrate (for peroxidase). The assay was performed according to the manufacturer's instructions (Biomedical Technologies, Mouse Osteocalcin EIA kit manual).

Briefly, the procedure involved a thawing of the supernatants obtained from the cell lysate preparation which had been stored at -20^{0}C. Osteocalcin protein standards (1.56, 3.12, 6.25, 12.5 and 50 ng/ml) were prepared from 50 ng stock solution (provided by the manufacturer) using the sample buffer. 25 µl of the blank (sample buffer), standards and thawed samples were pipetted into antibody-coated wells followed by the addition of 100 µl osteocalcin anti-serum in each well. The plate was then, incubated at 4^{0}C for 24 hrs. The wells were aspirated and washed 5 times with 0.3 ml/well phosphate saline wash buffer. 100 µl of streptavidin-horseradish peroxidase reagent was added to each well, swirled and incubated at room temperature for 30 minutes. Following the incubation period, the wells were washed as stated before. After complete washing, 100 µl of 3,3^1, 5,5^1- tetramethyl benzidine and hydrogen peroxide solution at ratio 1:1 was added to each well and incubated in the dark at room temperature for 15 minutes, after which 100 µl stop solution was added and the entire mixture, swirled. The absorbance was measured at 450 nm using Beckman Coulter AD-340 spectrophotometer (Beckman Coulter, Fullerton, CA). Concentrations of the protein were calculated based on the standard plot.

3.10 Anti-bacterial Activity

To evaluate the anti-bacterial activity of the samples, a colony of gram-positive *Streptococcus gordonii* was inoculated in 2 ml Bacto Todd-Hewitt broth (BD Biosciences, San Jose, CA) and this overnight culture was diluted 10 folds with 0.9% (w/v) NaCl solution. This was further diluted 50 folds with the Todd-Hewitt broth. Titanium discs (n=5) were placed into 24 well plate and 1ml of the diluted culture was added to each

well and incubated at 37^0C with mild shaking for 24 hrs. After the incubation period, the media was taken out and the discs were rinsed with 500 µl NaCl solution for 5 minutes. The discs were then, transferred to a new 24 well plate and washed thrice for 5 minutes with NaCl solution to remove any loosely adhered bacteria on the sides of the discs. After washing, 1 ml of the fresh Todd-Hewitt media was provided to each well containing the discs and incubated for 2 hrs. The incubation was undertaken to increase the metabolic activity of the bacteria and help them generate more adenosine triphosphate (ATP) so that the sensitivity of the ATP detection could be enhanced.

After the incubation period, the discs were washed thrice with the NaCl solution as described previously. After a complete washing, four discs per group were transferred into 1 ml centrifuge tube having 300 µl NaCl. These tubes were ultra-sonicated for 10 minutes to remove the bacteria adhered to the surface. One sample (which was not sonicated) per group was used for the SEM analysis.

3.11 Adenosine Triphosphate Quantification

The ATP quantification was performed using the BacTiter-Glo™ Microbial Cell Viability Assay kit (Promega, Madison, WI) in order to measure the metabolically active bacteria. This detection mechanism is based on the fact that mono-oxygenation of luciferin is catalyzed by luciferase enzymes in the presence of ATP, Mg^{2+}, and molecular oxygen. This reaction generates light (luminescence). The only source of ATP in this reaction is from the bacterial cells and hence, the amount of luminescence produced is directly proportional to the ATP in the cells, which in turn indicates the measure of metabolically active bacteria.

The procedure involved mixing 100 µl of the obtained solution after sonication and 100 µl of the BacTiter-Glo™ reagent in an opaque wall 96 well plate. After 5 minutes

of incubation at 37^0C, the luminescence was measured using BioTek microplate luminometer (BioTek, Winooski, VT).

3.12 Quantifying Colony Forming Units

While the ATP quantification gave us an estimate of the metabolic activity of the cells cultured in the samples, a measure of the colony forming units (CFUs) was expected to provide us the number of viable cells on the surface. When plated, each bacterial cell divided and formed visible colonies, which could be counted.

Briefly, the procedure involved diluting the 100 µl of the obtained solution, serially (10, 100, and 1000 folds). Then, 10 µl of the diluted and undiluted solutions were plated on the Todd-Hewitt Agar plates and incubated overnight at 37^0C in a humidified atmosphere of 5% CO_2. The number of CFUs was counted after the incubation period.

3.13 Scanning Electron Microscope (SEM)

In order to know the adhesion pattern of the bacteria on the surface of the coatings, samples were processed and viewed using the scanning electron microscope (SEM).

The discs were treated with a primary fixative (2% glutaraldehyde in 0.1M sodium cacodylate buffer, pH 7.4 with 0.15% alcian blue 8GX) for 1 hr at room temperature and then, kept at 4^0C, overnight. After the incubation period, the samples were washed with 0.1M cacodylate buffer for 5 minutes and treated with secondary fixative (1% OsO4/0.1M cacodylate buffer) for 1 hour. The samples were then, washed with 0.1M cacodylate buffer for 5 minutes and dehydrated with increasing ethanol concentrations {50%, 70%, 80%, 95% (twice), and 100% (twice)} for 5 minutes each.

After dehydration, the samples were critical point dried (CPD) with CO_2 and coated with 50Å platinum before being imaged on SEM.

3.14 Statistical Analysis

IBM SPSS Statistics version 19 (IBM, Armonk, NY) was used to perform the ANOVA (single factor), post-hoc tests (α=0.05), and the Levene's test. The Levene's test was used to assess the equality of variances between groups. Tukey's HSD post-hoc test was used for the groups having equal variances and Tamhane's T2 post-hoc test was used for the groups having unequal variances.

4. Experimental Plan

The flow chart (Figure 2) briefly describes the experimental plan of this work. First, the layers were built on the titanium surface using the LbL assembly, after which they were characterized / confirmed by contact angle measurements, DRIFTS, XPS, and AFM. The osteoblast cell adhesion and cell spreading studies were done on the LbL-modified surfaces. The samples were then, biomineralized by osteogenic media and analyzed by SEM, EDS, and DRIFTS. The osteoblast cell differentiation experiment was performed on the LbL-modified surfaces along with the biomineralized LbL-modified surfaces. Finally, the anti-bacterial activity of the LbL-modified surfaces against *S.gordonii* was analyzed using SEM and quantifying ATP and CFUs.

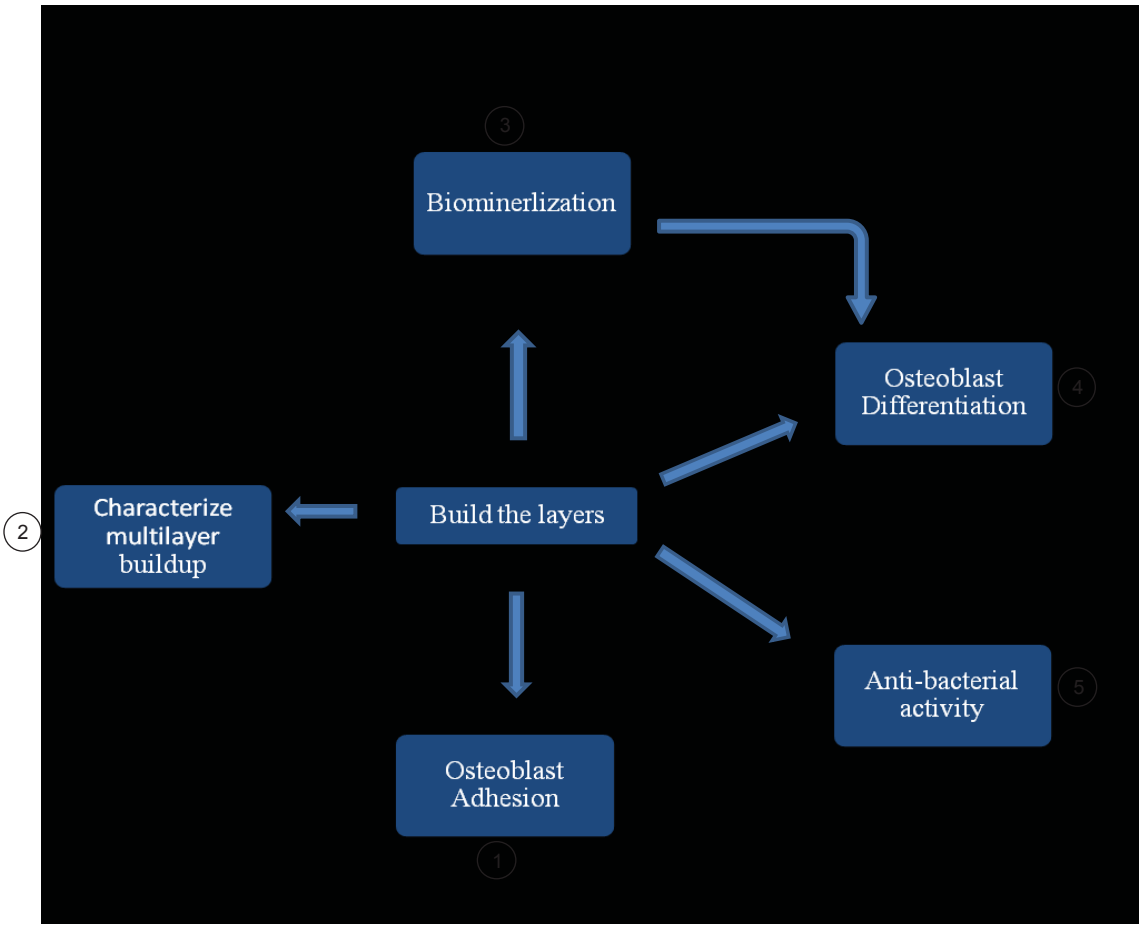

Figure 2: Experimental flow chart of the study

5. Results and Discussion

5.1 Layer-by-Layer Assembly

The LbL assembly of chitosan and the protein (P-HAP) on titanium was carried out at pH 4.5. Titanium is always covered with a few nanometers layers of titanium oxide which may be negatively charged at pH 4.5. By treating this with the chitosan solution, the cationic chitosan molecules (which were positively-charged at this pH) would get attracted electrostatically to form a layer (first layer). The samples were then, treated with the P-HAP solution which was anionic at pH 4.5. The electrostatic attraction between the chitosan and the P-HAP would drive the formation of a bi-layer. After each layer's adsorption, the samples were washed in water to remove any of the loosely adhered molecules. The samples were air-dried to remove the water molecules (which was adsorbed during the wash routine). The removal of the water molecules was important since both the molecules involved here (chitosan and P-HAP) were hydrophilic and could attract a layer of water molecules on their surface, which could hinder the multi-layer buildup. The water used for washing was also maintained at pH 4.5 so that the charge of the adsorbed molecules did not change and the electrostatic force of attraction was preserved. As the layers build-up, we would expect physical and chemical changes on the surface which were analyzed by various methods discussed below.

5.2 Contact Angle Measurement

The contact angle of the titanium surface was expected to change with the multi-layer buildup. This was because the outermost layer changes after each adsorption cycle as a result of which, the hydrophillicity of the surface changes. Figure 3 shows that the water contact of the untreated (plain) titanium surface was approximately 65^0. After

plasma cleaning, a significant drop to 8^0 was observed. The reason for this big drop in contact angle was because the plasma cleaning removed any contaminants on the surface and formed hydroxyl groups, which produced highly hydrophilic surfaces. After the adsorption of chitosan on the surface, the contact angle increased to approximately 60^0. This value was in accordance with previously reported contact angle values for chitosan adsorbed on titanium surface (15, 54, 60). After P-HAP was adsorbed following chitosan adsorption, there was a significant decrease ($p<0.05$) in the water contact angle (to approximately 22^0). The differences in the contact angle between each consecutive treatment (like between pTi and Ti+C, Ti+C and $(C+P)_1$ and so on) were statistically significant. There was no significant difference between the $(C+P)_1$ and the $(C+P)_2$ groups. Similarly, no significant difference was observed between the Ti+C and the $(C+P)_1C$ groups. It is therefore, clear that the outermost layer on the surface was changing as the layers continued to build up on the surface. Also, the contact angle was seen to not change significantly ($p>0.05$) when the groups having the same polymer as their outermost layer (like Ti+C and $(C+P)_1C$) were compared. This "zigzag" behavior of the contact angle during LbL assembly has been often reported (8,15, 54, 60, 67) and could be taken as one of the confirmation studies for the multi-layer buildup. Contact angle is a characteristic feature of the outermost layer and depends on the spreading of water droplet on the surface. In the absence of a uniform layer on the surface, say for example, if highly hydrophilic and hydrophobic component are unevenly distributed, the water molecules may prefer to move towards the hydrophilic component, thereby evading the hydrophobic component. In this case, since the water droplet would spread more, there could be a decrease in the contact angle. This factor may be attributed to a decrease in the contact angle in some of the studies involving LbL assembly (15, 54), where it has been reported that the contact angle was seen to decrease with the initial

increase of layers (for 4 layers) before displaying zigzag behavior. Those surfaces may have not been evenly covered by the polyions initially, and may have needed some layers for uniform layer adsorption. In this study, however, no such pattern was observed, which is indicative of uniform coating being present and displayed right from the very first layer.

While initially working on this multi-layer buildup, the drying (to remove water) between each adsorption was done with pressurized nitrogen gas. The contact angle results did not show any change between each of the adsorption cycles. Since the electrostatic interaction (between the positively-charged chitosan and the negatively-charged P-HAP molecules) are not that strong, it was assumed that the pressurized nitrogen gas had removed / disturbed the adsorbed layers during drying. This protocol was then, modified by just placing the samples under the chemical fume hood and allowing the water to evaporate, thus avoiding the use of pressurized gas. From the previous experiments, it was found that the evaporation time was approximately 10 minutes. So the samples were allowed to dry under the hood for 15 minutes after washing to make sure that the samples are free of any water molecules. The contact angle measurement decreased significantly when a batch of old chitosan (purchased a year ago) was used. This may be attributed to changes in chitosan's moisture content over time (68). After noticing this, a fresh batch of chitosan powder was obtained and used and this enabled the contact angle values to look similar to the values obtained in Figure 3.

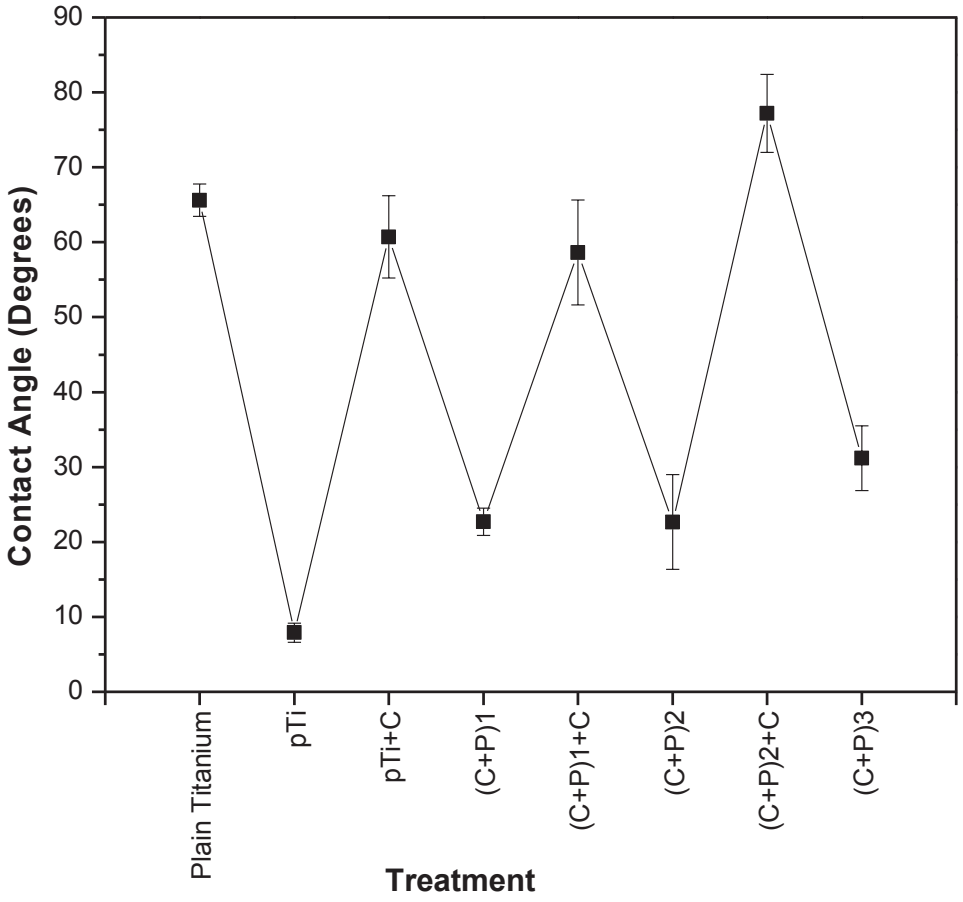

Figure 3: Contact Angle Measurements of plain titanium, pTi and LbL-modified surfaces

5.3 Diffuse Reflectance Fourier-transform infrared spectroscopy (DRIFTS)

The DRIFTS spectra collected for the multilayered samples are shown in Figure 4. Initially, the spectra for one bi-layered sample (with plasma-treated titanium) were analyzed to detect peaks which confirmed the presence of chitosan and P-HAP in order to substantiate the multi-layer buildup. The spectrum of the one bi-layered sample was no different from that of the plasma-treated titanium sample. This could be attributed to the fact that the penetration depth of DRIFTS is in the order of few micrometers. The thickness of one bi-layer in the LbL assembly would be in the range of a few nanometers

(58, 69). Hence, it is possible that the signal strength of the chitosan and P-HAP peaks were less intense and beyond the detection limit. As a result, visible spectral peaks for chitosan and the P-HAP were only observed upon addition of several layers (10 and 20 bi-layers) over the titanium surface.

The broad peak at around 3300 cm^{-1} which is seen in Figure 4 may be assigned to the O-H (present in chitosan) group and the N-H stretches (present in chitosan and P-HAP) (70,71,72,73). In addition, this broad peak around 3300 cm^{-1} can also be assigned to the O-H stretching in water (74,75). Moisture would have been absorbed on the surface during the multi-layer growth process. A couple of peaks in the region of 2900 cm^{-1} in Figure 4 may be attributed to the C-H stretch (70,72) which arises from both, the chitosan and the P-HAP molecules. The bands from 1650 to 1700 cm^{-1} (in Figure 4) may be attributed to the amide I vibration. The amide I band is generated due to the C=O stretching vibration, which is present in both, the chitosan and the P-HAP molecules (70, 71,73,76). The Amide II band at 1530 cm^{-1} (70, 71, 73, 76) can be noticed in the spectra, which is due to the NH bending vibration present in both the molecules. It is noted that the amide I and amide II bands can also be observed from the plasma-treated titanium surface, but the peaks collected for the multilayered surface (especially the 20 bi-layered surface) are stronger. The reason for the amide bands on the plasma-treated surface may be due to surface contamination during polishing/cleaning the samples. The CH_3 symmetric deformation which is characteristic of chitosan can be assigned to the peak shown in Figure 4 at around 1380 cm^{-1} (70,72). There are three peaks in the range of 1070 to 1250 cm^{-1}, which are due to C-N stretch (present in chitosan (70) and P-HAP), C-O-C stretch present in chitosan (70,71,73) and C-O stretching vibration (present in chitosan) (70,72,73).

In the LbL-modified surfaces, some of the peaks are unique to chitosan, but most of the bands obtained are common to both, the P-HAP and chitosan. Since both the molecules overlap structurally, it is often difficult to distinguish specific peaks. The ideal way of confirming the bi-layer formation would be to compare the spectrum of chitosan-coated plasma-treated titanium surface (one layer) and P-HAP + Chitosan (one bi-layer) coated plasma-treated titanium surface. Given the constraints which were explained earlier when collecting DRIFTS spectra for one bi-layered sample, this was deemed not feasible. However, the spectrum of 20 bi-layered surface corroborates the existence of both, chitosan and P-HAP in the layers coated over the titanium surface.

5.4 Atomic Force Microscopy (AFM)

The surface topographies of Chitosan / P-HAP LbL-modified surfaces were analyzed using the tapping mode AFM (Figure 5). The uncoated plasma-treated titanium surface displayed a smooth topography whereas the LbL-modified surfaces (one and ten bi-layers) showed granular structures which were evident from the two-dimensional and three-dimensional images (Figure 5). The granular structures observed here were seen in several LbL Assemblies reported in literature (14,15,33,54,77). The size of these granules increased with the number of bi-layers (granules on the ten bi-layer surface were considerably larger when compared with one bi-layered surface). This kind of granular growth in LbL assembly had been reported previously (77). From Figure 6, however, it became clear that the average roughness (R_a) increased as the number of bi-layers increased and this suggests that the height of the granules present in ten bi-layered samples was greater than that of the initial granules present in the one bi-layered sample. The R_a of all the three surfaces were statistically different ($p<0.05$) from each other.

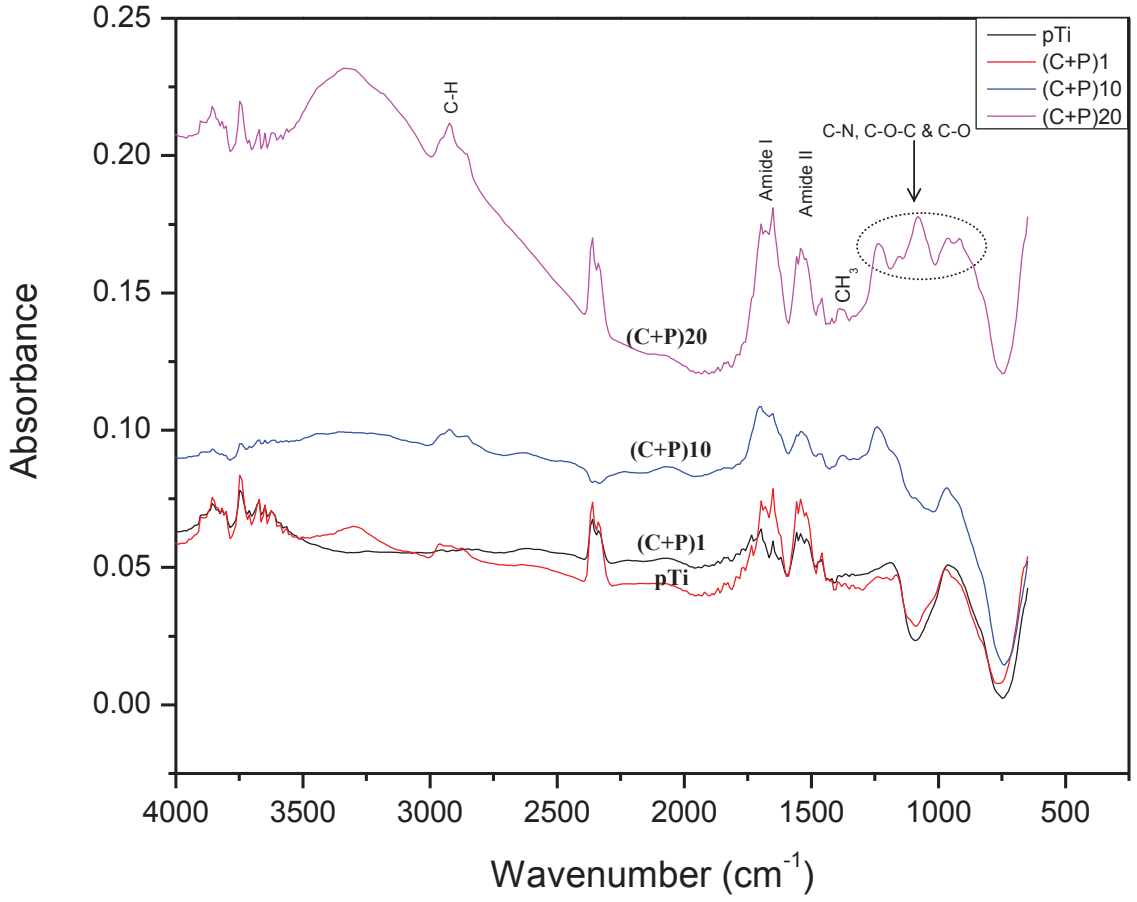

Figure 4: DRIFTS spectra of pTi and LbL-modified surfaces

The granular structures present in the LbL-modified surfaces could be attributed to the characteristic behavior of P-HAP molecule which was observed in a previous study involving LbL assembly of P-HAP and chitosan on a glass surface (33). However, the granular structures seen in that study were visible only when the multi-layered samples were maintained above the inverse transition temperature (ITT) of P-HAP, which was around 33^0C. It has been reported that above the ITT, the polymer side

chains of P-HAP changes its conformation (33). This results in the formation of aggregates, which is visualized as granular structures on the surface. In our study, the multi-layers were built at room temperature which was below the ITT of the P-HAP. Although the temperature (around 25^0C) at which the multi-layers were built was less than the ITT of the P-HAP, significant turbidity (due to the formation of aggregates) was observed in the P-HAP solution used. We used water to dissolve the P-HAP, whereas 0.15M NaCl solution (pH 5) was used in the reported study (33). The difference in the ionic strength of the solutions could have caused this difference in the ITT. This would have caused a decrease in the ITT. The decrease in ITT was well-detected because of the turbidity observed in the P-HAP solution. Since both the molecules (chitosan and P-HAP) electrostatically attracted each other, one molecule would have been surrounded by another resulting in the growth of these granular structures. As the number of bi-layers increased, the height of these granules would also increase. The initial granules formed on the one bi-layered sample would have combined with one another in the LbL process, making the granules increase in size along with the increased numbers of layers. Hence, the increase in the average roughness could correspond very well to the granular structures present in Figure 5.

The surface area difference (S.A.D) of the samples is listed in Table 2. The S.A.D of the ten bi-layered samples was found to be greater than that of the plasma-treated titanium samples, but was less than that of one bi-layered sample. The S.A.D of all the three surfaces were statistically different ($p<0.05$) from each other. Considering the equation for the S.A.D, the increase in the value was due to the increase in the surface area of the granules. Since there were no granules in the plasma-treated titanium samples, its S.A.D would naturally be the least. While comparing the one to the ten bi-layered samples, the number of granules was found to be substantially higher in

that one bi-layer. The surface area of such small, but numerous granules would be higher than a few big granules (observed in ten bi-layered surface) which could be the reason for such high S.A.D in one bi-layered surface.

Table 2: Surface area difference (%) of pTi and LbL-modified surfaces calculated from AFM images

Treatment	Surface Area Difference (%)
pTi	0.67±0.15
$(C+P)_1$	4.64±0.63
$(C+P)_{10}$	2.38±0.26

5.5 X-Ray Photoelectron Microscopy (XPS)

XPS is a surface-sensitive technique which offers information about the elemental composition of the surface. The nitrogen-containing groups are present in both, chitosan and P-HAP, but absent in plasma-treated titanium surface. These nitrogen-containing groups which were specific to chitosan and P-HAP were used as indicators to confirm the deposition of bi-layers on the surface. Figure 7 shows the spectra of the pTi and LbL-modified titanium {$(C+P)_1$, $(C+P)_{10}$ and $(C+P)_{20}$}. The pTi shows three elements, namely titanium, carbon, and oxygen. The binding energies are 458eV and 463.6eV for titanium (Ti 2p3/2 and Ti 2p1/2 respectively). For oxygen and carbon, the corresponding values are 531eV and 285eV respectively. The titanium and oxygen peaks were due to the presence of titanium oxide layer on the surface.

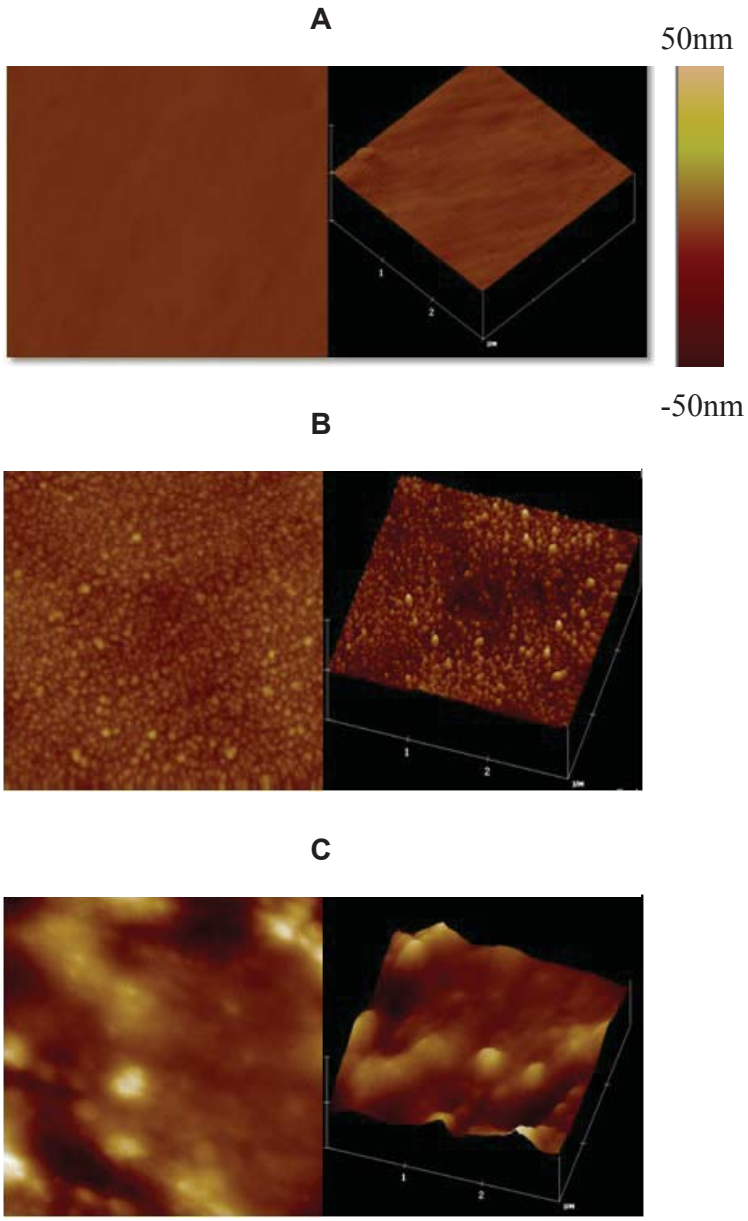

Figure 5: AFM images of pTi and LbL-modified surfaces. **(A)** pTi surface **(B)** One bi-layered surface **(C)** Ten bi-layered surface. The image on the left and the right shows two-dimensional and three-dimensional pictures.

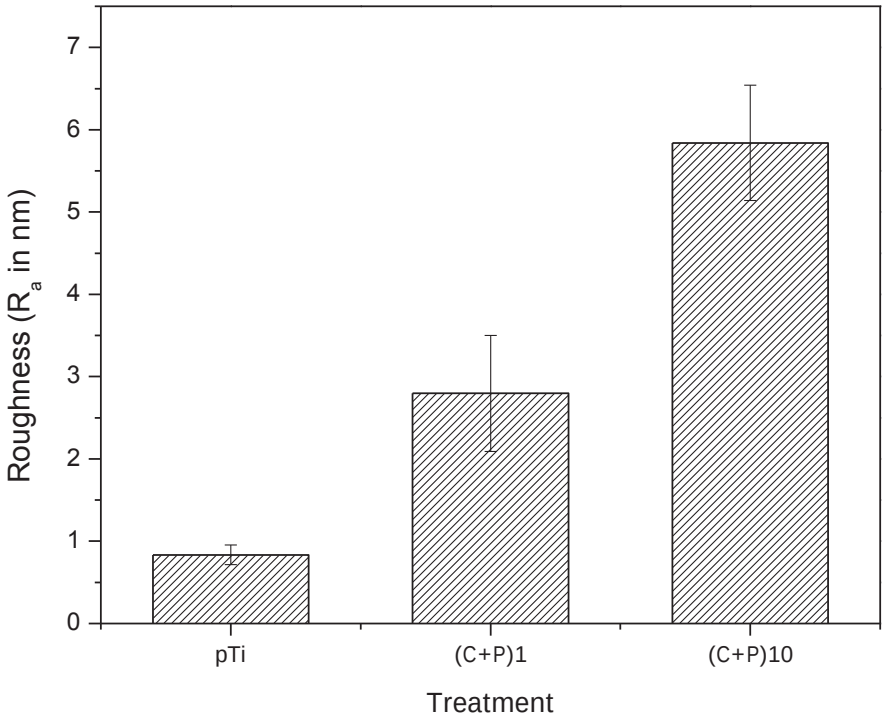

Figure 6: Average Roughness data of pTi and LbL-modified surfaces calculated from AFM images

Carbon's presence could be attributed commonly to the surface contamination (15). In the LbL-modified surface, the nitrogen peak emerged due to the number of nitrogen atoms present in chitosan and P-HAP molecules. It is important to also note that the titanium peak disappeared in all LbL-modified surfaces, even in the case of one bi-layer. This indicates that the surface was completely covered by chitosan and P-HAP molecules starting from the very first bi-layer. Given the penetration depth of XPS and the area from the which the electrons were extracted (from around 5 nm depth (78)), it may be inferred that each bi-layer covered a minimum of 5 nm on the titanium. This result was a strong indication confirming the buildup of layers during the LbL assembly.

This kind of elemental interpretation using XPS for LbL assembly has also been reported elsewhere (8,14, 15, 54).

5.6 Characterization of Biominerlization

The ability of the LbL-modified and unmodified (pTi) titanium samples to induce calcium phosphate mineralization was analyzed by template-directed mineral formation (79) which used an osteogenic medium. The osteogenic medium was supplemented with fetal bovine serum (FBS), calcium chloride, and β-glycerophosphate. The calcium ions were electrostatically attracted to the surface having P-HAP (having high negative charge). The alkaline phosphatase enzyme (present in FBS) hydrolyzed the β-glycerophosphate and released the phosphate ions. These negatively-charged phosphate ions bound to calcium ions on the surface and as the calcium phosphate minerals increased in size, they consumed the newly enzyme-liberated phosphate ions. Thus, the amount of calcium phosphate mineralization should be directly proportional to the surface's bioactivity. The formation of calcium phosphate minerals on the implant surface is the key in osteoblast cell differentiation which ultimately leads to the bone formation around the implant (22,23,24).

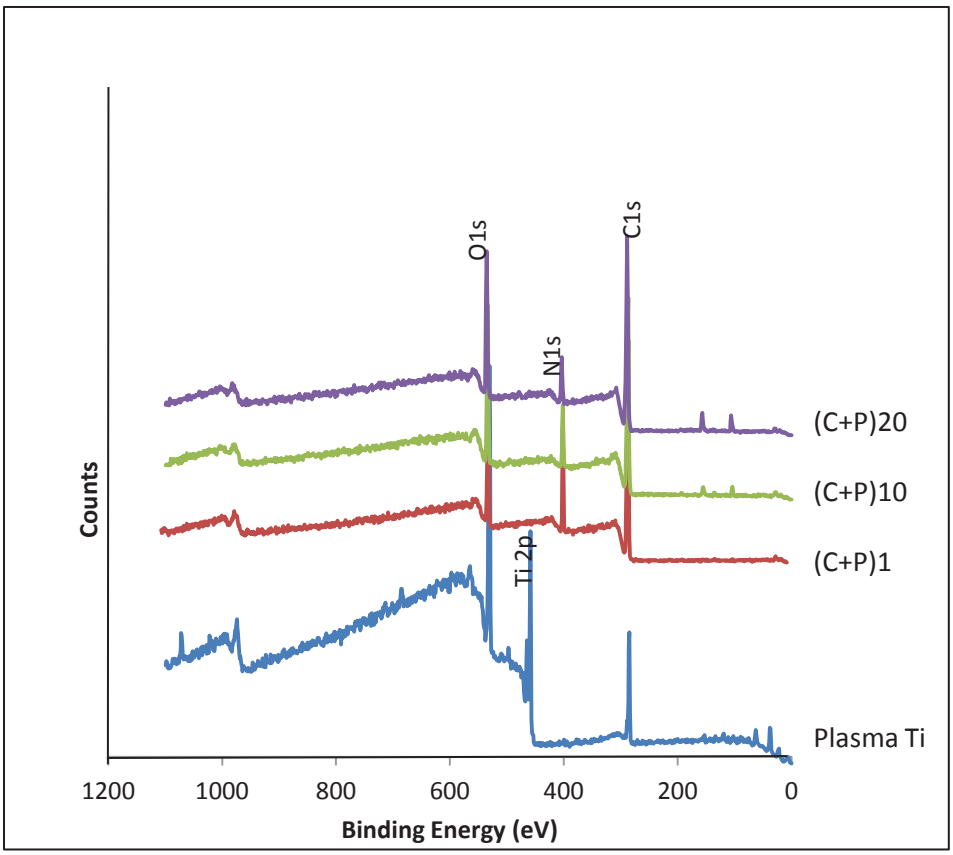

Figure 7: XPS spectra of pTi and LbL-modified surfaces

5.6.1 Diffuse Reflectance Fourier-transform infrared spectroscopy (DRIFTS)

The DRIFTS spectra of the biomineralized samples are shown in Figure 8. The broad peak at around 3300 cm^{-1} confirms the presence of the O-H stretch in water (74, 75). Water could have been incorporated during multi-layer buildup and from the osteogenic medium. Two peaks at around 2900 cm^{-1} (C-H stretch) which were observed in Figure 4 can still be seen in Figure 8. The amide I and II peaks were also visible in the biomineralized samples.

The weak peak at around 1380 cm^{-1} (CH_3 symmetric deformation) which appears in Figure 4 almost disappears when the samples are biomineralized. This may be attributed to the formation of a thick calcium phosphate mineral layer on the surface. The C-N, C-O-C and C-O stretching vibrations which were observed in Figure 4 were not observed here. Instead of this, a broad peak was observed from 900 to 1170 cm^{-1}. This peak corresponding to the biomineralized samples was due to the overlapping of the P-O symmetric and anti-symmetric stretching vibrations (74,75,80,81, 82, 83, 84, 85, 86) of the PO_4 groups in phosphate. It may also be seen that the strength of the DRIFTS signal increased substantially as the number of bi-layers increased, which is an indication that the amount of mineralization increased with the increased number of bi-layers. The peak at 863 cm^{-1} was attributed to the carbonate group present in the calcium phosphate minerals which was normally reported in the biomineralization process (74,81,84,87). However, as the phosphate peak intensified with the increase in the number of bi-layers, the carbonate peak did not intensify. This spectrum (Figure 8) could be deemed a characteristic of amorphous calcium phosphate precipitation on the surface (74,75,83,84). Although there are other peaks (Amide I and Amide II) which can be attributed to the P-HAP in the spectra of biomineralized samples, it is also important to take into consideration the precipitation of several proteins on the surface as derived from osteogenic media. Since the peaks are generic for all the proteins, we cannot distinguish between the P-HAP and the osteogenic media protein peaks. The disappearance of chitosan-specific CH_3 peak gives an inference that the minerals will fully cover the surface, making the chitosan molecules inaccessible to the infrared rays.

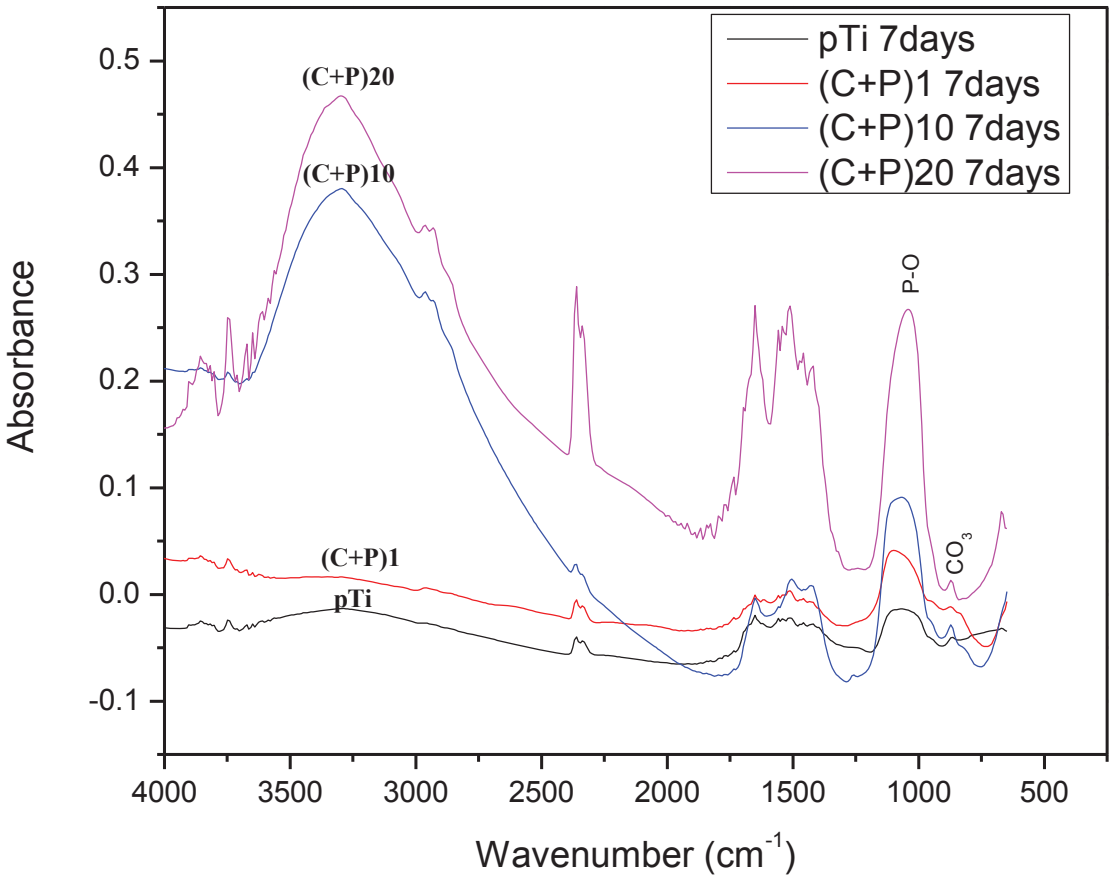

Figure 8: DRIFTS spectra of the biomineralized pTi and LbL-modified surfaces

5.6.2 Scanning Electron Microscope (SEM) andEnergy Dispersive X-ray Spectroscopy (EDS)

The calcium phosphate minerals were formed on all the surfaces which can be visualized in SEM pictures (Figure 9) after 7 days of incubation in osteogenic media. In the case of LbL-modified surfaces, these minerals seem to be in abundance. The highest amount of mineral accumulation was observed for $(C+P)_{20}$, followed by $(C+P)_{10}$, $(C+P)_{1,}$ and pTi respectively. It was noted that the minerals on the one bi-layered surface ($(C+P)_1$) were growing on a previously developed and homogeneously formed mineral

layer. This pattern was also observed on other LbL-modified surfaces (ten and twenty bi-layers). However, this kind of mineralization pattern was not observed in the case of pTi, where the minerals were randomly distributed on the bare titanium surface. The minerals on the pTi surface could be due to non-specific and random precipitation of calcium and phosphate ions from osteogenic media. It was clear from the SEM pictures that the amount of mineral deposition increased with the number of bi-layers on the surface. The reason for the increased amount of mineralization could be attributed to the increased amount of P-HAP as the number of bi-layers increased, and these would have attracted many calcium and phosphate ions. It is well known that Hydroxyapatite (HA) is the major mineral component in bones. The calcium to phosphate ratio (Ca/P) of HA (formula = $Ca_5(PO_4)_3(OH)$ is 1.67. The Ca/P ratio was estimated for the bio-mineralized samples in order to know how close these formed calcium phosphate minerals were to HA, stoichiometrically. EDS (coupled with SEM) was used to find this Ca/P ratio and the values have been listed in Table 3. The ratio of the formed minerals on the LbL-modified surface were close to that of hydroxyapatite (Ca/P ratio = 1.67). The Ca/P ratio of the plasma-treated titanium could not be detected by EDS since the mineralization was very low (as seen in the SEM pictures). The mineralization process was specific to the fetal bovine serum (FBS) used in the osteogenic media. When the FBS source was changed, mineralization was not observed. This indicates the importance of FBS in this process. The exact reason for this complete shift in mineralization in unclear as the manufacturers do not seem to have given the complete specification about their serum. While FBS contains many proteins which can be specific to the manufacturer, this change in mineralization results may be attributed to the alteration in these proteins (especially alkaline phosphatase) which can affect the mineralization process.

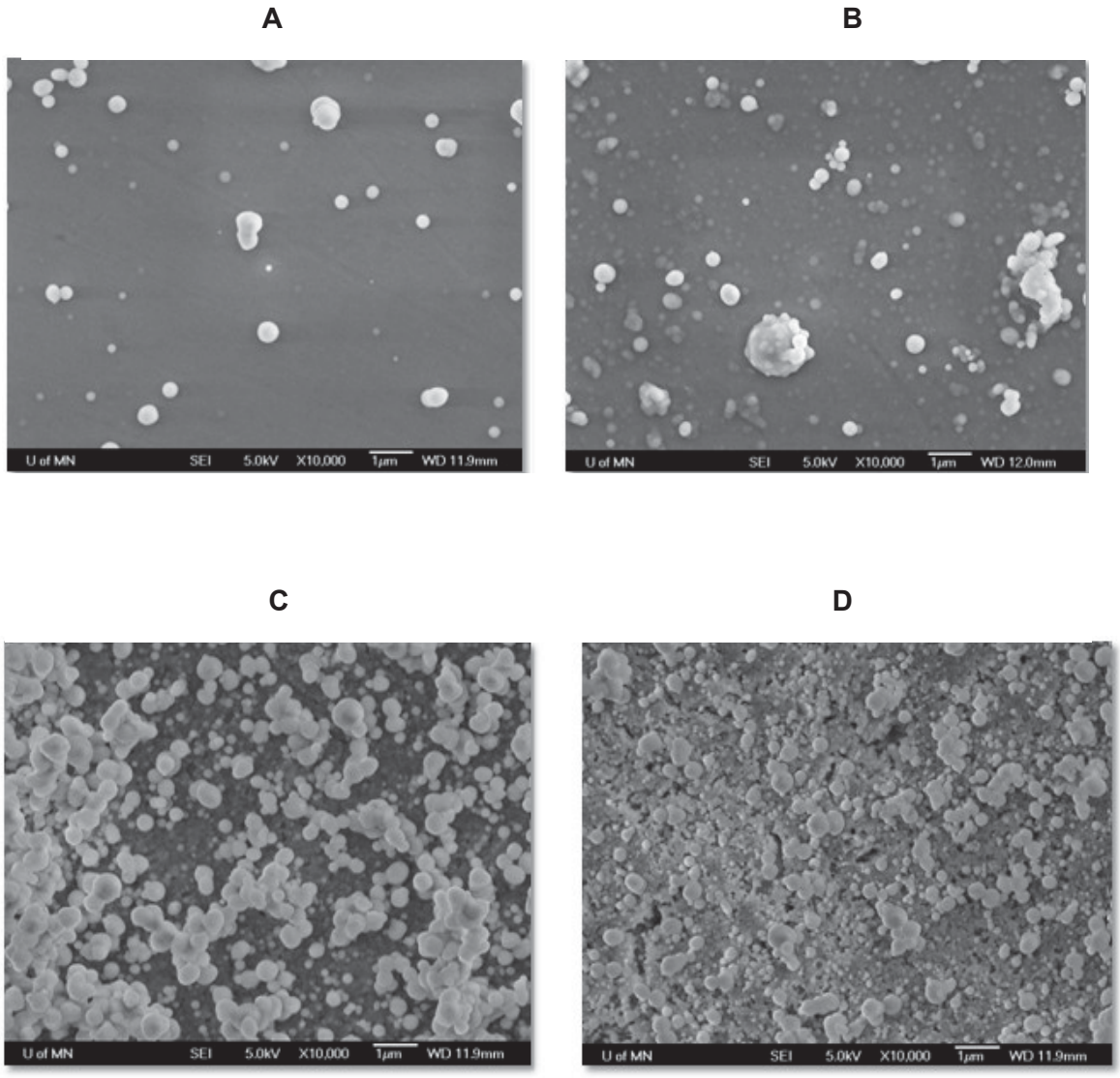

Figure 9: SEM pictures of biomineralized pTi and LbL-modified surfaces. **(A)** pTi **(B)** One bi-layered surface, **(C)** Ten bi-layered surface, and **(D)** Twenty bi-layered surface.

Table 3: Calcium to phosphate ratio of the biomineralized surfaces calculated by EDS

Treatment	Ca/P Ratio (Atomic)
(C+P)1 - 7days BM	1.56±0.14
(C+P)10 - 7days BM	1.56±0.09
(C+P)20 - 7days BM	1.62±0.06

5.7 Osteoblast Cell Experiments

Osteoblast cells have been studied extensively because of key role in bone formation (7,10,11,14,17,22,23,88,89). Factors such as, adhesion, spreading, and differentiation of osteoblast cells which are known to greatly affect bone matrix formation(7,11, 90) have been analyzed in this study. As more cells initially adhered and spread to the implant surface, there would be an increased amount of bone-matrix deposition. When the pre-osteoblasts differentiate and become mature cells, they start to involve in the bone formation from extracellular matrix (91,92). As the time needed for this differentiation step reduces, so also does the time for bone formation around the implant.

5.7.1 Cell Adhesion and Spreading

The immunofluoresence staining in Figure 10 shows that the TCPS, pTi, and Ti+C promote good osteoblast cell-spreading. Chitosan is known to promote osteoblast adhesion and spreading (93) because of its structural similarity towards glycosaminoglycans (GAGs) (55). Since GAGs are constituents of cell surface and

extracellular matrix (94), they participate in cell adhesion, proliferation and differentiation (95, 96). TCPS is the positive control for cell adhesion and spreading. The pTi has a coating of oxide layer which imparts high surface energy. High surface energy enhances protein adsorption which can lead to good cell adhesion and spreading (10, 97). It is important to note that when P-HAP is incorporated (in one bi-layer), there was a decrease in cell spreading. When the number of bi-layers increased on the surface, the cells did not spread well and were circular in shape. This kind of poor spreading has been observed previously (10). The reason for this may be due to the surface becoming less rigid because of the significant accumulation of polymer layers (chitosan and P-HAP). Since osteoblast cells are used to rigid surfaces (bone matrix – where the cells predominantly live), they prefer titanium surface which is more rigid than the LbL modified surfaces. An extensive study on the rigidity of the surface with respect to differentiation has also been reported (98) wherein the less rigid surfaces did not direct osteoblast differentiation. It may be noted that even when the outermost layer was covered with chitosan in LbL coatings {$(C+P)_{10}C$ and $(C+P)_{20}C$}, the cellular spreading remained very poor, while Ti+C showed good spreading. This may be because the presence of only chitosan adsorbed on titanium surface may still prompt the cells to sense the rigidity of the titanium surface. This rigidity may have reduced later as the number of bi-layers deposited increased. Though there were no statistically significant changes in the number of adhered cells between the treatments (Figure 11), however, it may be observed that as the number of bi-layers increased, the number of adhered cells also increased. The reason for this trend may be due to the increased number of anchoring points (owing to the presence of chitosan) on the LbL-modified surface. The increased number of adhered cells on the surface is an indication that the LbL-modified surfaces are cytocompatible.

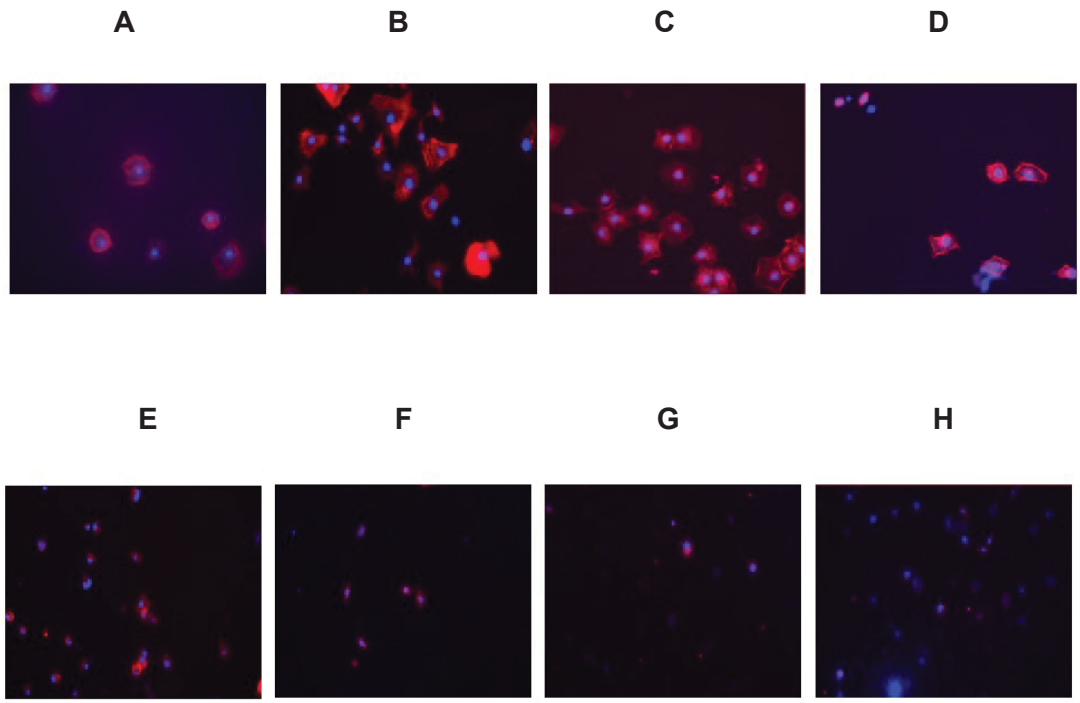

Figure 10: Cell spreading images of osteoblast cells cultured on TCPS, pTi and LbL-modified surfaces. **(A)** TCPS **(B)** Plasma-treated titanium, **(C)** Ti+C (D) One bi-layered surface **(E)** Ten bi-layered surface **(F)** Ten bi-layered surface with chitosan as outermost layer **(G)** Twenty bi-layered surface **(H)** Twenty bi-layered surface with chitosan as outermost layer

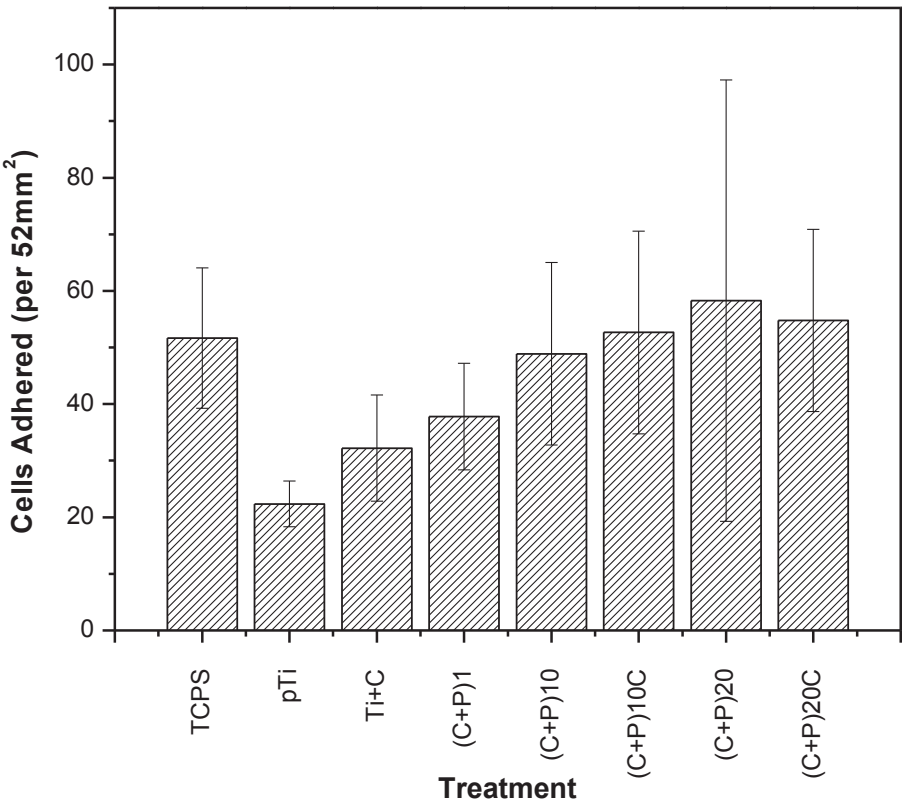

Figure 11: Cell adhesion study of osteoblast cultured on TCPS, pTi and LbL-modified surfaces.

5.7.2 Cell Differentiation

Alkaline Phosphatase (ALP) activity is an early osteoblast differentiation marker. As seen in Figure 12, LbL modification on the titanium surface did not show improvement in the ALP activity (normalized with total protein content). In fact, by looking closely at the 14th day data, the ALP activity was seen to be low in higher number of bi-layers except for the $(C+P)_{20}$ treatment. The ALP activity (14th day) of the $(C+P)_{20}C$ treatment was significantly low ($p<0.05$) when compared to TCPS, pTi, and Ti+C treatments. Also, the 14th day ALP activity of $(C+P)_{10}$ treatment was significantly

lower ($p<0.05$) than the TCPS and the Ti+C treatments. The ALP activity of all other treatments were statistically non-significant ($p>0.05$).

Osteocalcin is known to be a late differentiation marker for osteoblast cell differentiation. The amount of osteocalcin released from the cells quantified by EIA and normalized with total protein content is shown in Figure 13. Here, the LbL modification significantly decreased the amount of osteocalcin expressed by the cells. The osteocalcin expression on the 21st day of the treatment $(C+P)_{10}$ C was significantly lower ($p<0.05$) than that of TCPS, pTi, and Ti+C treatments. Treatments $(C+P)_{10}$ and $(C+P)_{20}C$ also showed significant reductions in osteocalcin expression when compared to the TCPS and Ti+C treatments. Also, the osteocalcin expression of the $(C+P)_{20}$ treatment was lower than that of Ti+C treatment. The Ti+C treatment showed results similar to those of the TCPS and pTi. There was no significant difference between these treatments ($p>0.05$). The TCPS, pTi, and the Ti+C groups were the ones which favored cell spreading and other groups which had multi-layers did not allow the cells to spread. The increase in the number of bi-layers did not make the cells spread and differentiate well. It was clear from the biomineralization studies that the LbL assembly greatly increased the accumulation of calcium phosphate minerals. But when it came to cell differentiation, it showed a negative effect. This may be driven by the fact that the cells initially adhered to the surface of the titanium discs, which would have prevented the biomineralization process. As the formation of calcium phosphate minerals on the surface heavily relies on the surface charge of surface (explained in biomineralization (section 2)), the blocking by the cells may have hindered this process. The time needed for cell adhesion was just 4 hrs when compared to the formation of calcium phosphate minerals, which was around 7 days. From this analysis, it may be seen that the cells

adhered to the surface and covered most of the spaces even before the commencement of mineralization.

As the non-mineralized samples were not driving the osteoblast differentiation, the biomineralized LbL modified titanium surfaces were analyzed for their abilities to provide biochemical cues for differentiation. Figure 14 shows the ALP activity of the LbL modified biomineralized samples. The ALP activity on the 7^{th} day of TCPS was significantly higher than that of pTi, biomineralized pTi, and biomineralized $(C+P)_{10}$ treatments. However, there were no significant differences between the other treatments on the 14^{th} day and 21^{st} day time points. It was clear that even when the LbL treated titanium surfaces were covered with the minerals, the driving force for osteoblast differentiation was found lacking.

The cell experiments were repeated with some procedural changes. The titanium discs used in the previous experiments were small (area= 28.3 mm^2) when compared to the size of the wells (area = 78.5 mm^2). So, the sizes of the discs were increased (area = 63.6 mm^2) in order to have more cells adhere to the disc surface instead of the TCPS surface (bottom of the well). Also, in order to test the effect of lower chitosan concentration, 0.1 mg/ml of chitosan was used (compared to 1 mg/ml used earlier). This group was named (C+P)1*. The hypothesis was that, if we had low chitosan concentrations, then, we would have a greater number of free, active groups from P-HAP. These groups may have been involved in the electrostatic interaction with chitosan molecule, which could have prevented their access to the cells. The samples were collected only on days 14 and 21 as there was no significant ALP activity on day 7 (from the results of our previous experiments). Also, another conclusion from the previous experiments was that the osteocalcin expression was significant only on day 21. Keeping these in mind, the ALP activity was analyzed for samples from days 14 and 21

and the osteocalcin expression was quantified for the 21st day samples. The ALP activity and osteocalcin measurements have been shown in Figures 15 and 16 respectively. In spite of the procedural tweaking, the data was no different from those derived from the previous experiments and the LbL modification did not show any effect on osteoblast differentiation.

The mineralization clearly increased with the number of bi-layers, which is evident from Figure 9. The biochemical cues which were provided by these minerals could be masked by the mechanical property (stiffness) of the minerals/LbL assembly. The optimal elastic modulus for osteoblast differentiation is around 30-40kPa (98). The elastic moduli of the LbL modified surfaces are unknown, but the modulus of the materials used -- titanium, chitosan (99), and minerals (100) are significantly higher. The elastic modulus of P-HAP is not known. As the elastic modulus played an important role in driving cellular differentiation (98), there is a high probability that the modulus of the LbL modified surfaces would be substantially different than the optimal elastic modulus for osteoblast differentiation. Apart from this, the Chitosan-P-HAP interaction and the dissociation products of P-HAP could have contributed to this kind of poor osteoblast differentiation response.

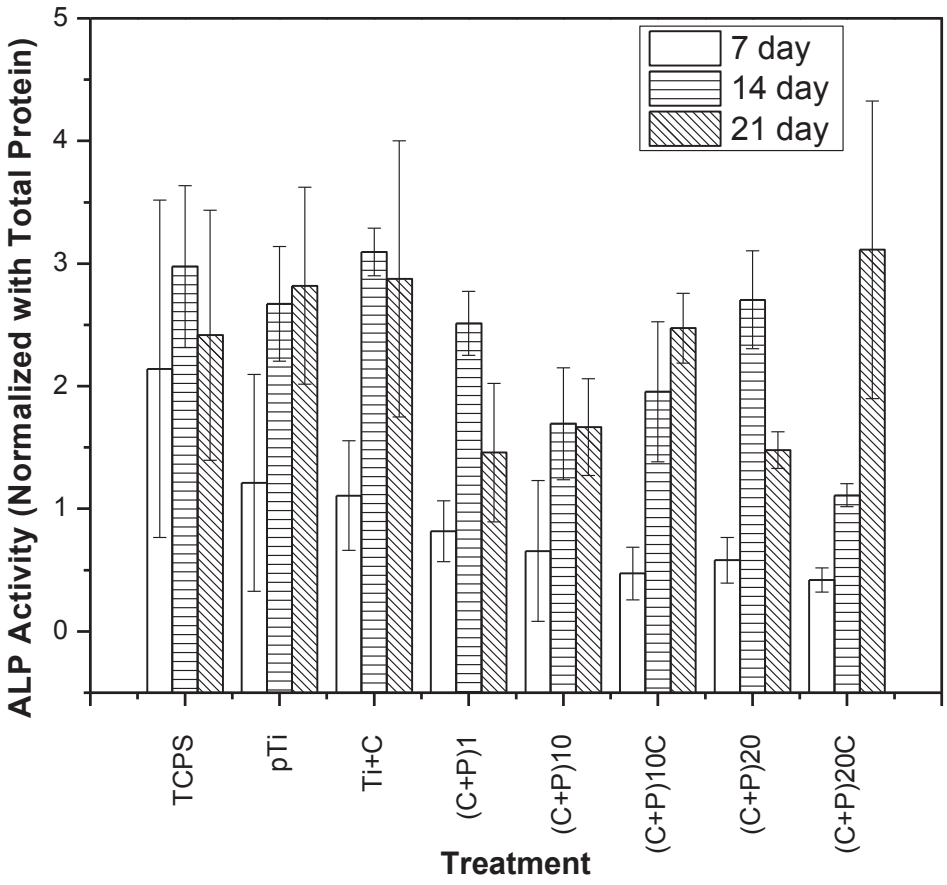

Figure 12: ALP activity of osteoblast cells cultured on TCPS, pTi and LbL-modified surfaces. The ALP activity was normalized with the total protein content of each sample.

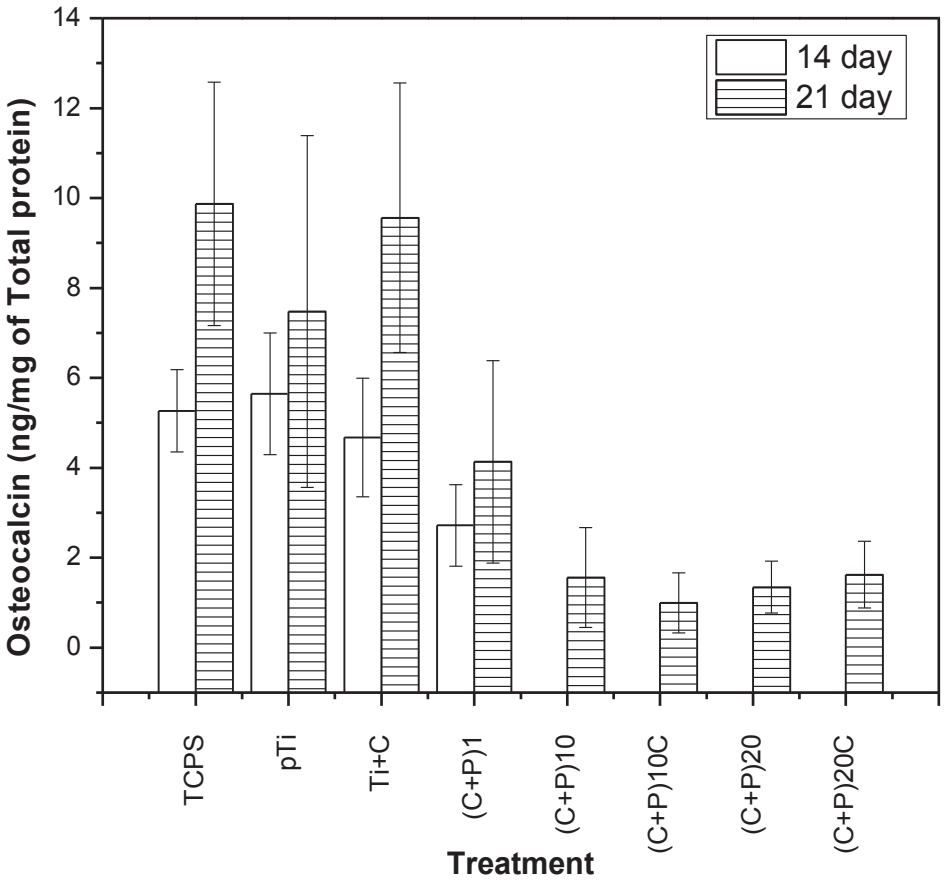

Figure 13: Osteocalcin expression of osteoblast cells cultured on TCPS, pTi and LBL modified surfaces. The osteocalcin quantity was normalized with the total protein content of each sample.

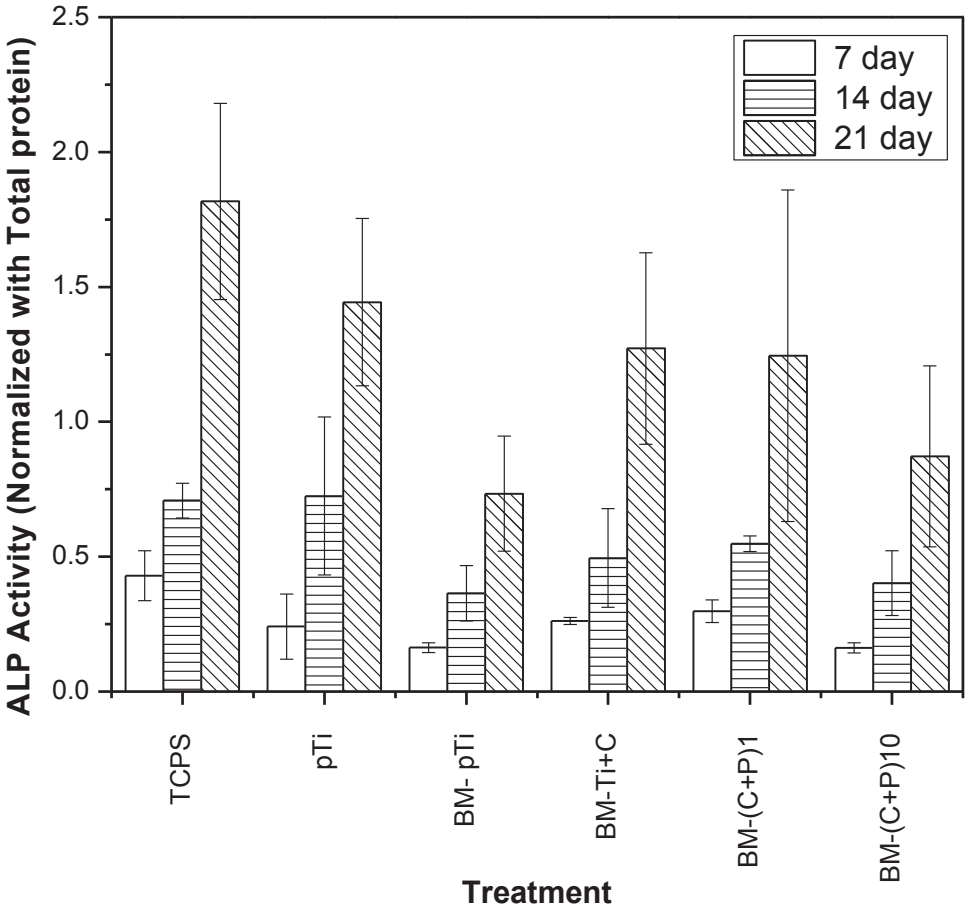

Figure 14: ALP activity of osteoblast cells cultured on TCPS, pTi and biomineralized (BM) LbL- modified surfaces. The ALP activity was normalized with the total protein content of each sample.

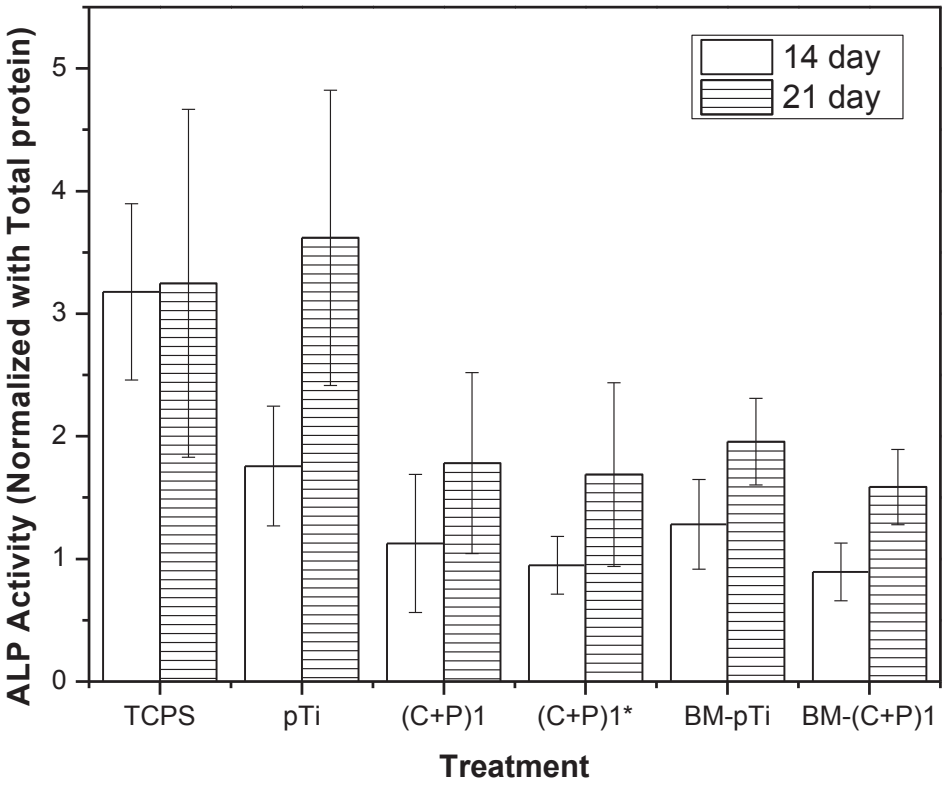

Figure 15: ALP activity of osteoblast cells cultured on TCPS, pTi titanium and biomineralized (BM) LbL-modified surfaces after procedural modifications. The ALP activity was normalized with the total protein content of each sample. (C+P)1* - LbL assembly with 0.1 mg/ml chitosan)

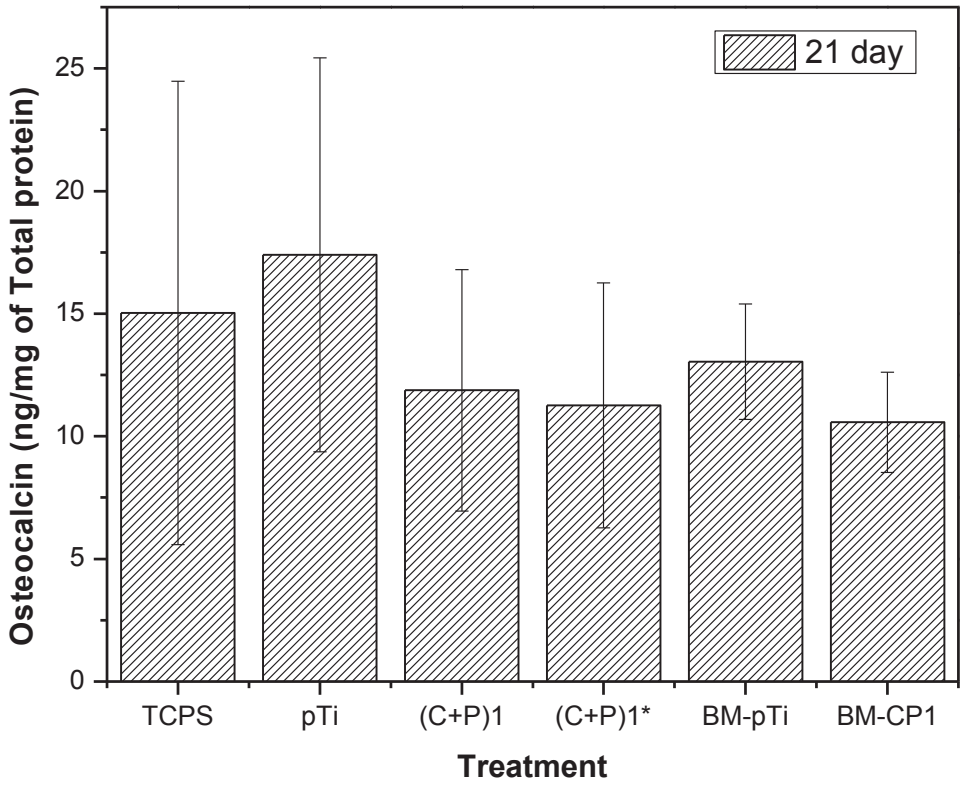

Figure 16: Osteocalcin expressed by osteoblast cells cultured on TCPS, pTi and LbL-modified surfaces after procedural modifications. The osteocalcin quantity was normalized with the total protein content of each sample. (C+P)1*- LbL assembly with 0.1 mg/ml chitosan)

5.8 Anti-bacterial Activity

The gram positive *Streptococcus gordonii*'s response towards the LbL modified surfaces was also analyzed. Colony forming units (CFU) and ATP activity of the bacteria reduced significantly in all the LbL modified surfaces (Figure 17). Even the surface with one layer of chitosan (Ti+C) showed great reduction demonstrating the anti-bacterial efficacy of the chitosan layer. The number of viable bacteria was reduced to at least 50

fold in the case of LbL- modified surfaces (based on CFU/ml). The CFU/ml of the LbL modified surfaces (Ti+C, $(C+P)_1$, $(C+P)_{10}$ and $(C+P)_{10}C$) was found to be significantly lower ($p<0.05$) than that of pTi. In a stress environment, the bacteria could possibly be viable but would perhaps be in a dormant state with low metabolic activity. Since the ATP and CFU data were highly correlated ($r=0.99$), it confirmed that the reasons for low metabolic activity (ATP) in LbL modified surfaces was because of less viable bacteria present on the surface (resulting in lower CFU/ml). It was expected that the number of amine groups (responsible for anti-bacterial activity) would increase with the number of bi-layers, which will ultimately enhance the anti-bacterial activity. In this study, the anti-bacterial activity was independent of the number of bi-layers and did not increase with the number of bi-layers. The reason for not having such a response could be attributed to the amine groups which would have been involved in the ionic bonding with P-HAP during LbL assembly and thus reduce the number of active groups.

The SEM pictures (Figure 18) show that bacterial adhesion reduced as a result of LbL modification. This confirms that the reduced ATP and CFU values were a result of less bacteria adhering to the surface. To clarify if P-HAP played any role in reduced bacterial adhesion, P-HAP was adsorbed on plasma-treated samples and was tested against *S.gordonii*. As seen in Figures 19 and 20, the SEM images and ATP values of the surface coated with P-HAP was the same as that of the plasma-treated titanium surface, suggesting that the anti-bacterial effect caused by LbL modified surfaces was primarily due to chitosan. Generally, it is believed that the chitosan acts as an anti-bacterial agent by attracting the bacteria towards it and disturbing the cell wall dynamics (5,44,49,50,51). Contrary to this hypothesis, the LbL treated surfaces (even with chitosan as outermost layer) did not show increased bacterial adhesion when compared to the pTi surface. This led to the conclusion that chitosan was anti-adhesive to the

bacteria rather than bactericidal. Peri-implantitis is caused by the colonization of pathogenic organisms like *Phorphyromonas gingivalis*. The early colonizers (like *S.gordonii*) prepare the environment for the late colonizers which usually need highly demanding growth conditions (101). *P.gingivalis,* which is a late colonizer is known to bind itself with the early colonizers like *S.gordonii* (102) and thereby colonize the implant's surface via biofilm formation. By reducing the number of adherent *S.gordonii* on the implant surface, the surface will be less prone to infectious organisms like *P.gingivalis*. This would reduce the risk of peri-implantitis after implantation.

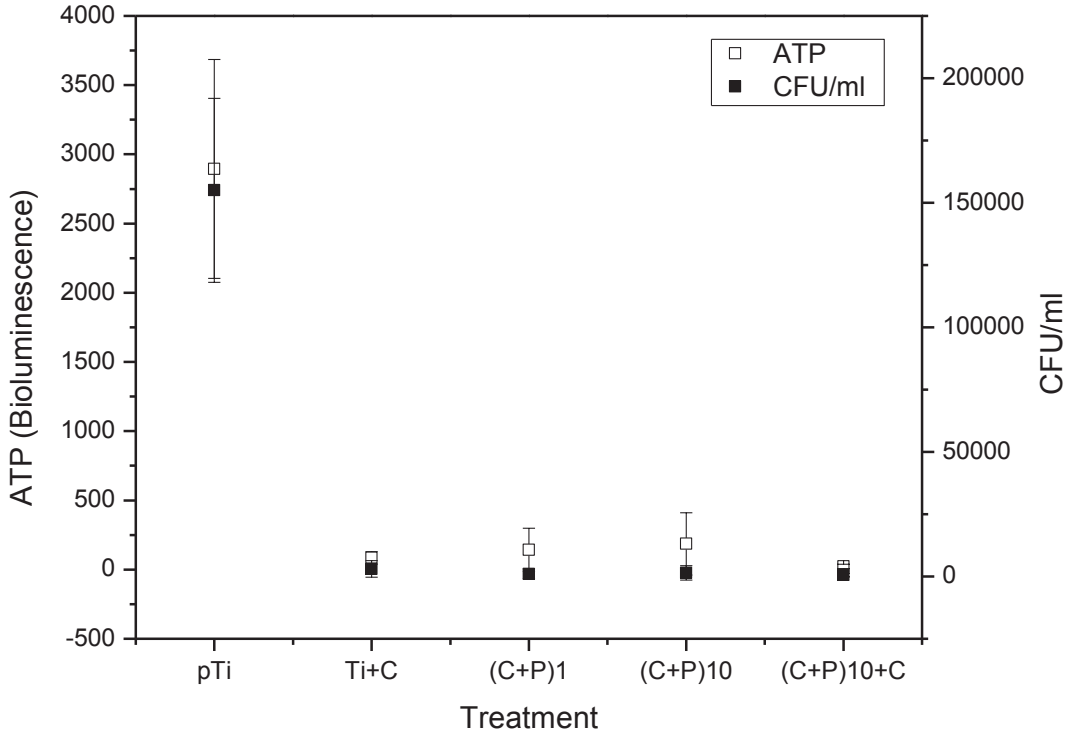

Figure 17: ATP and CFU of *S. gordonii* cultured on pTi and LbL-modified surfaces

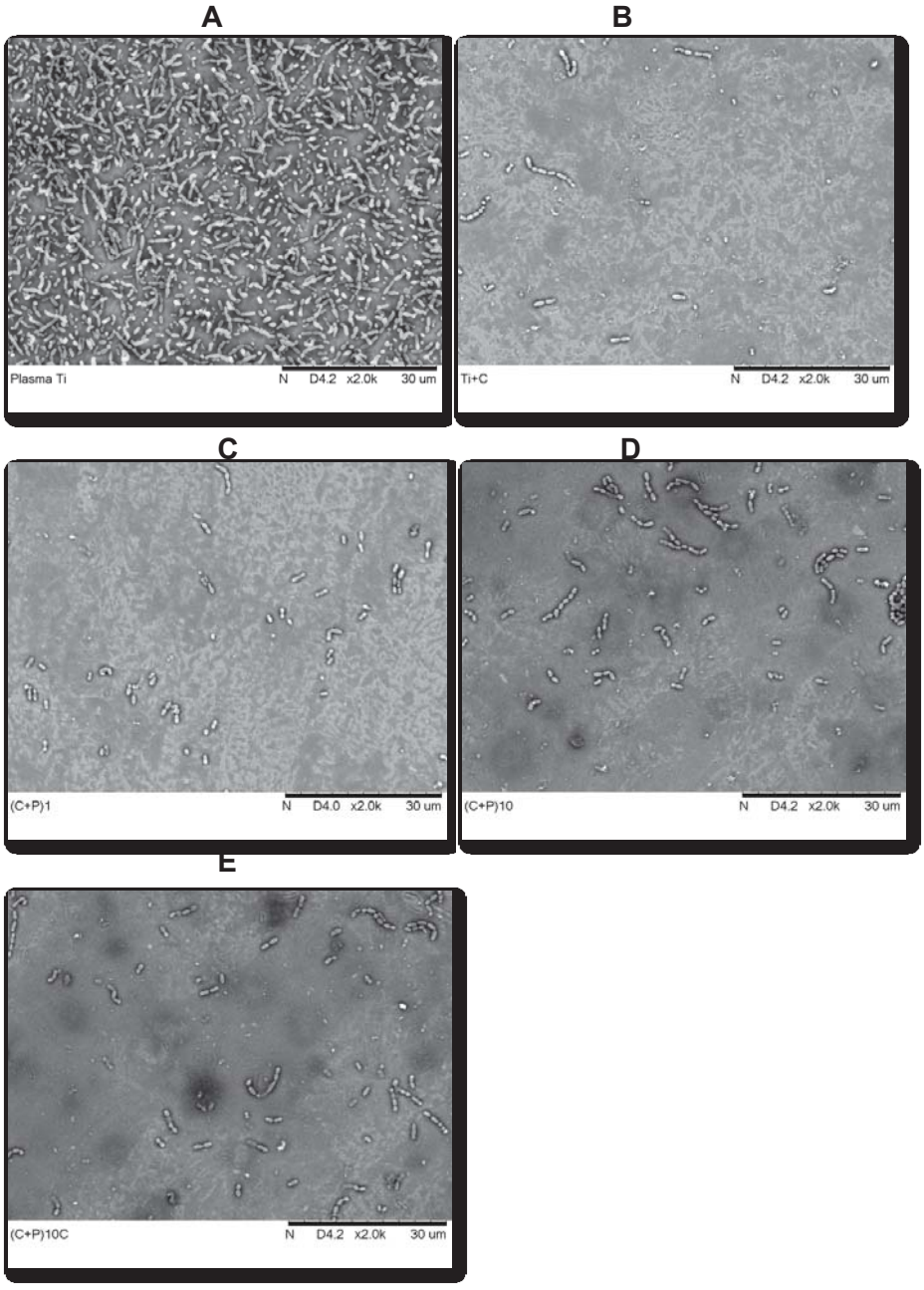

Figure 18: SEM pictures of *S. gordonii* attached to pTi and LbL-modified surfaces. **(A)** pTi **(B)** Ti+C **(C)** One bi-layered surface **(D)** Ten bi-layered surface **(E)** Ten bi-layered surface with chitosan as outermost layer.

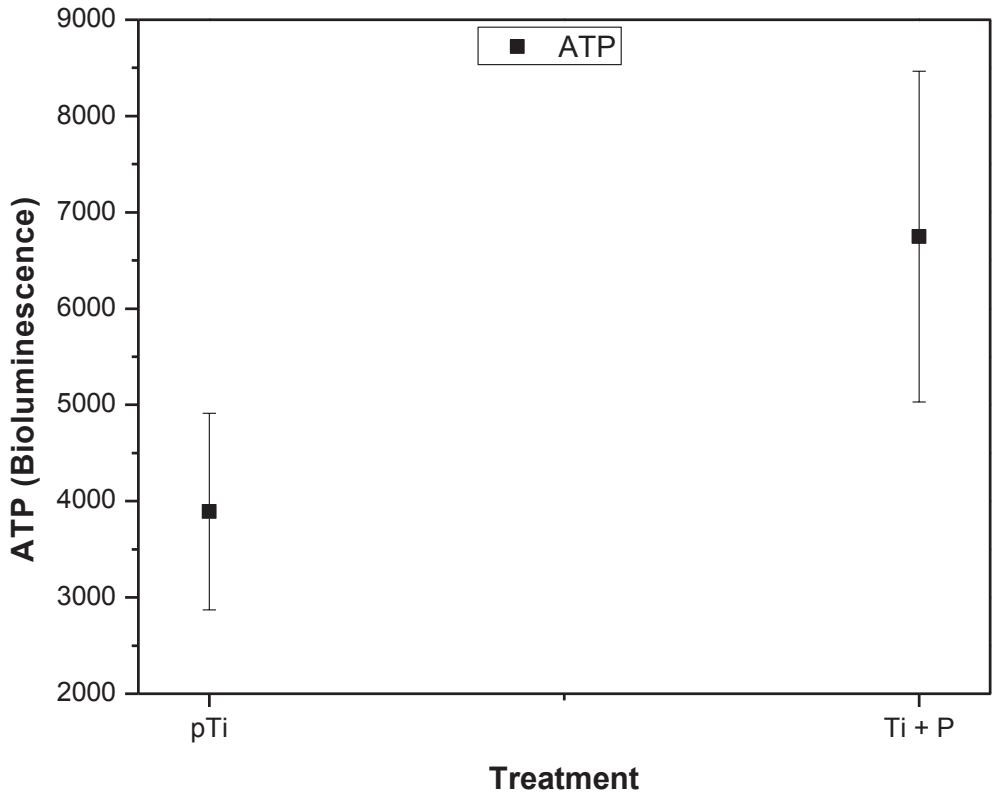

Figure 19: ATP of *S. gordonii* cultured on pTi and P-HAP coated surfaces

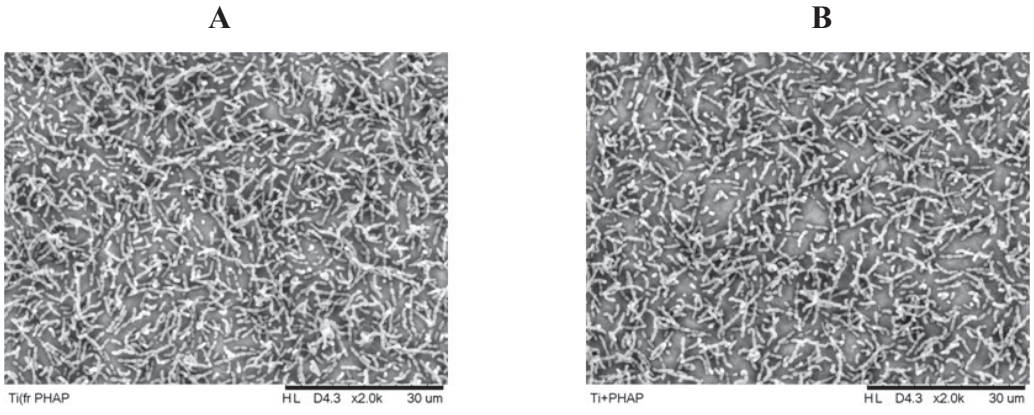

Figure 20: SEM pictures of *S.gordonii* attached to pTi and P-HAP coated surfaces. (A) pTi (B) Ti+P-HAP

.

6. Conclusions

The Chitosan/P-HAP bi-layers were successfully built on the titanium surface using the Layer-by-Layer technique. The layers have been characterized by contact angle measurements, AFM, XPS, and DRIFTS.

The DRIFTS spectra along with the SEM-EDS data confirms that the LbL-modification induces the surface to form calcium phosphate mineral which is stoichiometrically close to that of the Ca/P ratio of amorphous hydroxyapatite. Also, the amount of mineralization substantially increased with the increase in the number of bi-layers.

The LbL- modified surfaces were cytocompatible to mouse pre-osteoblast cells and effective against *S.gordonii* as it showed a 50 fold decrease in the number of viable bacteria (based on colony forming units) when compared to pTi with no bi-layer.

However, the LbL modified surface did not influence the osteoblast cell differentiation as expected, in spite of its ability to induce biomineralization. This may be due to the lack of rigidity of the obtained bi-layers coating titanium (98), and further studies are necessary to confirm this hypothesis.

7. Future Work

The layers were built based on electrostatic attraction and hence, there would be a question about the structural integrity of the LbL assembly. During the surgical placement of the implant, we can expect the layers to be disturbed if the layers are not strongly adhered to the surface. Hence, in future studies, assessing the mechanical stability using ultra-sonication should give an idea about the stability of layers on the titanium surface. If the contact angle value of the LbL assembly changes significantly after it is ultra-sonicated, then it is an indication that the layers are not strongly attached to the surface. This can be a quick and simple approach to evaluate the mechanical stability of the layers. If they are not structurally stable, utilizing chemical cross-linking using 1-ethyl-3-(3-dimethylaminopropyl) carbodiimide (EDC) and *N*-hydroxysulfo succinimide (NHS) (103) will be a good strategy to reinforce them. This bonding is based on the formation of amide bond between carboxylic and amine groups of the polymers involved in the LbL assembly. This cross-linking chemistry, apart from stabilizing the layers, has also been proved to be cytocompatible (103). After this coupling, evaluating the biomineralization and anti-bacterial properties of the LbL-modified surfaces will reveal whether the LbL assemblies retain their properties.

Measuring the elastic modulus of the developed LbL assembly (Chitosan/P-HAP) as well as the biomineralized - LbL assembly surface will give us an idea of how close these values are to the optimal modulus for osteoblast differentiation (30-40KPa). This can validate our hypothesis that the poor osteblast differentiation observed in this study was due to the rigidity factor associated with the surfaces.

In this study, the anti-bacterial activity of the LbL-modified surfaces was analyzed using *S.gordonii*, which is an early colonizer. It would be ideal if the surfaces can be

analyzed with a co-culture of early (like *S.gordonii*) and late colonizers (like *P.gingivalis*). This would actually mimic the natural environment surrounding the implant (104). Also, the anti-bacterial activity of the biomineralized LbL-modified surfaces should be analyzed. This will help us to know if the LbL assembly will be effective against bacteria even when it is covered by minerals.

8. References

1. O'Brien M, Kaczor M. 2011 Orthopedic Outlook. William Blair & Company [Internet]. [cited 2012 Jun 24]; Available from: http://www.acgchicago.com/UserFiles/file/chicago/Web%20docs/HCare%202011%20Orthopedic%20HCare.pdf

2. 2004 Orthopedic Industry Outlook: 15% revenue growth to $20 billion. ORTHOPEDIC AND DENTAL INDUSTRY NEWS [Internet]. 2003 Dec 15 [cited 2012 Jun 24]; Available from: http://www.healthpointcapital.com/research/2003/12/15/2004_orthopedic_industry_outlook_15_revenue_growth_to_20_billion/

3. Norowski PA Jr, Bumgardner JD. Biomaterial and antibiotic strategies for peri-implantitis: a review. J. Biomed. Mater. Res. Part B Appl. Biomater. 2009 Feb;88(2):530–43.

4. Schliephake H, Scharnweber D. Chemical and biological functionalization of titanium for dental implants. Journal of Materials Chemistry. 2008;18(21):2404.

5. Klinge B, Hultin M, Berglundh T, others. Peri-implantitis. Dental Clinics of North America. 2005;49(3):661–76.

6. Fischer K, Stenberg T, Hedin M, Sennerby L. Five-year results from a randomized, controlled trial on early and delayed loading of implants supporting full-arch prosthesis in the edentulous maxilla. Clinical oral implants research. 2008;19(5):433–41.

7. Le Guéhennec L, Soueidan A, Layrolle P, Amouriq Y. Surface treatments of titanium dental implants for rapid osseointegration. Dental materials. 2007;23(7):844–54.

8. Chua PH, Neoh KG, Shi Z, Kang ET. Structural stability and bioapplicability assessment of hyaluronic acid-chitosan polyelectrolyte multilayers on titanium substrates. Journal of Biomedical Materials Research Part A. 2008 Dec 15;87A(4):1061–74.

9. Kong L, Gao Y, Lu G, Gong Y, Zhao N, Zhang X. A study on the bioactivity of chitosan/nano-hydroxyapatite composite scaffolds for bone tissue engineering. European Polymer Journal. 2006 Dec;42(12):3171–9.

10. Chua PH, Neoh KG, Kang ET, Wang W. Surface functionalization of titanium with hyaluronic acid/chitosan polyelectrolyte multilayers and RGD for promoting osteoblast functions and inhibiting bacterial adhesion. Biomaterials. 2008;29(10):1412–21.

11. Chesnutt BM, Yuan Y, Buddington K, Haggard WO, Bumgardner JD. Composite chitosan/nano-hydroxyapatite scaffolds induce osteocalcin production by osteoblasts in vitro and support bone formation in vivo. Tissue Eng Part A. 2009 Sep;15(9):2571–9.

12. Aparicio C, Gil FJ, Fonseca C, Barbosa M, Planell JA. Corrosion behaviour of commercially pure titanium shot blasted with different materials and sizes of shot particles for dental implant applications. Biomaterials. 2003 Jan;24(2):263–73.

13. Albrektsson T, Jacobsson M. Bone-metal interface in osseointegration. J Prosthet Dent. 1987 May;57(5):597–607.

14. Cai K, Hu Y, Jandt KD, Wang Y. Surface modification of titanium thin film with chitosan via electrostatic self-assembly technique and its influence on osteoblast growth behavior. Journal of Materials Science: Materials in Medicine. 2007 Jul 10;19(2):499–506.

15. Cai K, Rechtenbach A, Hao J, Bossert J, Jandt KD. Polysaccharide-protein surface modification of titanium via a layer-by-layer technique: Characterization and cell behaviour aspects. Biomaterials. 2005 Oct;26(30):5960–71.

16. Länge K, Herold M, Scheideler L, Geis-Gerstorfer J, Wendel H-P, Gauglitz G. Investigation of initial pellicle formation on modified titanium dioxide (TiO2) surfaces by reflectometric interference spectroscopy (RIfS) in a model system. Dent Mater. 2004 Nov;20(9):814–22.

17. Müller R, Abke J, Schnell E, Scharnweber D, Kujat R, Englert C, et al. Influence of surface pretreatment of titanium- and cobalt-based biomaterials on covalent immobilization of fibrillar collagen. Biomaterials. 2006 Aug;27(22):4059–68.

18. Nanci A, Wuest JD, Peru L, Brunet P, Sharma V, Zalzal S, et al. Chemical modification of titanium surfaces for covalent attachment of biological molecules. J. Biomed. Mater. Res. 1998 May;40(2):324–35.

19. Aparicio C, Manero JM, Conde F, Pegueroles M, Planell JA, Vallet-Regí M, et al. Acceleration of apatite nucleation on microrough bioactive titanium for bone-replacing implants. Journal of Biomedical Materials Research Part A. 2007 Sep 1;82A(3):521–9.

20. Csucs G, Michel R, Lussi JW, Textor M, Danuser G. Microcontact printing of novel co-polymers in combination with proteins for cell-biological applications. Biomaterials. 2003 May;24(10):1713–20.

21. LeGeros RZ. Calcium Phosphate-Based Osteoinductive Materials. Chemical Reviews. 2008 Nov 12;108(11):4742–53.

22. Shu R, McMullen R, Baumann MJ, McCabe LR. Hydroxyapatite accelerates differentiation and suppresses growth of MC3T3-E1 osteoblasts. J Biomed Mater Res A. 2003 Dec 15;67(4):1196–204.

23. Okumura M, Ohgushi H, Dohi Y, Katuda T, Tamai S, Koerten HK, et al. Osteoblastic phenotype expression on the surface of hydroxyapatite ceramics. J. Biomed. Mater. Res. 1997 Oct;37(1):122–9.

24. Jarcho M. Calcium phosphate ceramics as hard tissue prosthetics. Clin. Orthop. Relat. Res. 1981 Jun;(157):259–78.

25. Piattelli A, Cosci F, Scarano A, Trisi P. Localized chronic suppurative bone infection as a sequel of peri-implantitis in a hydroxyapatite-coated dental implant. Biomaterials. 1995;16(12):917–20.

26. Johnsson M, Levine MJ, Nancollas GH. Hydroxyapatite binding domains in salivary proteins. Critical Reviews in Oral Biology & Medicine. 1993;4(3):371–8.

27. Raj PA, Johnsson M, Levine MJ, Nancollas GH. Salivary statherin. Dependence on sequence, charge, hydrogen bonding potency, and helical conformation for adsorption to hydroxyapatite and inhibition of mineralization. J. Biol. Chem. 1992 Mar 25;267(9):5968–76.

28. Rodríguez-Cabello JC, Martín L, Girotti A, García-Arévalo C, Arias FJ, Alonso M. Emerging applications of multifunctional elastin-like recombinamers. Nanomedicine. 2011;6(1):111–22.

29. Roy MD, Stanley SK, Amis EJ, Becker ML. Identification of a Highly Specific Hydroxyapatite-binding Peptide using Phage Display. Advanced Materials. 2008 May 19;20(10):1830–6.

30. Zhang R, Ma PX. Biomimetic Polymer/Apatite Composite Scaffolds for Mineralized Tissue Engineering. Macromolecular Bioscience. 2004 Feb 20;4(2):100–11.

31. Rodríguez-Cabello JC, Prieto S, Arias FJ, Reguera J, Ribeiro A. Nanobiotechnological approach to engineered biomaterial design: the example of elastin-like polymers. Nanomedicine. 2006;1(3):267–80.

32. Rodríguez-Cabello JC, Martín L, Alonso M, Arias FJ, Testera AM. “Recombinamers” as advanced materials for the post-oil age. Polymer. 2009;50(22):5159–69.

33. Barbosa JS, Costa RR, Testera AM, Alonso M, Rodríguez-Cabello JC, Mano JF. Multi-Layered Films Containing a Biomimetic Stimuli-Responsive Recombinant Protein. Nanoscale Research Letters. 2009 Jul 16;4(10):1247–53.

34. Rodríguez-Cabello JC, Reguera J, Girotti A, Arias FJ, Alonso M. Genetic Engineering of Protein-Based Polymers: The Example of Elastinlike Polymers. In: Vancso GJ, editor. Ordered Polymeric Nanostructures at Surfaces [Internet]. Berlin/Heidelberg: Springer-Verlag; [cited 2012 Jun 24]. p. 119–67. Available from: http://www.springerlink.com/index/10.1007/12_047

35. Joshi RI, Eley A. The in-vitro effect of a titanium implant on oral microflora: comparison with other metallic compounds. Journal of medical microbiology. 1988;27(2):105–7.

36. Leonhardt A, Renvert S, Dahlén G. Microbial findings at failing implants. Clin Oral Implants Res. 1999 Oct;10(5):339–45.

37. Yoshinari, Oda Y, Kato T, Okuda K. Influence of surface modifications to titanium on antibacterial activity in vitro. Biomaterials. 2001;22(14):2043–8.

38. Ghandour W, Hubbard JA, Deistung J, Hughes MN, Poole RK. The uptake of silver ions by Escherichia coli K12: toxic effects and interaction with copper ions. Applied microbiology and biotechnology. 1988;28(6):559–65.

39. Chen W, Liu Y, Courtney HS, Bettenga M, Agrawal CM, Bumgardner JD, et al. In vitro anti-bacterial and biological properties of magnetron co-sputtered silver-containing hydroxyapatite coating. Biomaterials. 2006 Nov;27(32):5512–7.

40. Kälicke T, Schierholz J, Schlegel U, Frangen TM, Köller M, Printzen G, et al. Effect on infection resistance of a local antiseptic and antibiotic coating on osteosynthesis implants: An in vitro and in vivo study. Journal of Orthopaedic Research. 2006 Aug;24(8):1622–40.

41. Stigter M, De Groot K, Layrolle P. Incorporation of tobramycin into biomimetic hydroxyapatite coating on titanium. Biomaterials. 2002 Oct;23(20):4143–53.

42. Stigter M, Bezemer J, De Groot K, Layrolle P. Incorporation of different antibiotics into carbonated hydroxyapatite coatings on titanium implants, release and antibiotic efficacy. Journal of Controlled Release. 2004 Sep 14;99(1):127–37.

43. Campbell AA, Song L, Li XS, Nelson BJ, Bottoni C, Brooks DE, et al. Development, characterization, and anti-microbial efficacy of hydroxyapatite-chlorhexidine coatings produced by surface-induced mineralization. J. Biomed. Mater. Res. 2000;53(4):400–7.

44. Raafat D, Von Bargen K, Haas A, Sahl H-G. Insights into the Mode of Action of Chitosan as an Antibacterial Compound. Applied and Environmental Microbiology. 2008 May 2;74(12):3764–73.

45. Rabea EI, Badawy ME-T, Stevens CV, Smagghe G, Steurbaut W. Chitosan as Antimicrobial Agent: Applications and Mode of Action. Biomacromolecules. 2003 Nov;4(6):1457–65.

46. An YH, Farino M, Kang QK, Demcheva MV, Vournakis J. Glucosamine Coating for Inhibiting Bacterial Adhesion to Titanium Surfaces. Key Engineering Materials. 2005;288-289:343–6.

47. Ikinci, Senel S, Akincibay H, Kaş S, Erciş S, Wilson CG, et al. Effect of chitosan on a periodontal pathogen Porphyromonas gingivalis. International Journal of Pharmaceutics. 2002;235(1-2):121–7.

48. Chung Y-C, Wang H-L, Chen Y-M, Li S-L. Effect of abiotic factors on the antibacterial activity of chitosan against waterborne pathogens. Bioresour. Technol. 2003 Jul;88(3):179–84.

49. Chung Y, Su Y, Chen C, Jia G, Wang H, Wu JCG, et al. Relationship between antibacterial activity of chitosan and surface characteristics of cell wall. Acta Pharmacol. Sin. 2004 Jul;25(7):932–6.

50. Kim S-K, Rajapakse N. Enzymatic production and biological activities of chitosan oligosaccharides (COS): A review. Carbohydrate Polymers. 2005 Dec 14;62(4):357–68.

51. Helander IM, Nurmiaho-Lassila EL, Ahvenainen R, Rhoades J, Roller S. Chitosan disrupts the barrier properties of the outer membrane of gram-negative bacteria. Int. J. Food Microbiol. 2001 Dec 30;71(2-3):235–44.

52. Choi BK, Kim KY, Yoo YJ, Oh SJ, Choi JH, Kim CY. In vitro antimicrobial activity of a chitooligosaccharide mixture against Actinobacillus actinomycetemcomitans and Streptococcus mutans. Int. J. Antimicrob. Agents. 2001 Dec;18(6):553–7.

53. Kim JY, Lee JK, Lee TS, Park WH. Synthesis of chitooligosaccharide derivative with quaternary ammonium group and its antimicrobial activity against Streptococcus mutans. International Journal of Biological Macromolecules. 2003 Mar;32(1–2):23–7.

54. Cai K, Hu Y, Jandt KD. Surface engineering of titanium thin films with silk fibroin via layer-by-layer technique and its effects on osteoblast growth behavior. Journal of Biomedical Materials Research Part A. 2007 Sep 15;82A(4):927–35.

55. Francis Suh J-K, Matthew HW. Application of chitosan-based polysaccharide biomaterials in cartilage tissue engineering: a review. Biomaterials. 2000 Dec 15;21(24):2589–98.

56. Decher G. Fuzzy Nanoassemblies: Toward Layered Polymeric Multicomposites. Science. 1997 Aug 29;277(5330):1232–7.

57. Sohn B-H, Kim T-H, Char K. Process-Dependent Photocatalytic Properties of Polymer Thin Films Containing TiO 2 Nanoparticles: Dip vs Spin Self-Assembly Methods. Langmuir. 2002 Oct;18(21):7770–2.

58. Zheng L, Yao X, Li J. Layer-by-Layer Assembly Films and their Applications in Electroanalytical Chemistry. Current Analytical Chemistry. 2006;2(3):279–96.

59. Croll TI, O'Connor AJ, Stevens GW, Cooper-White JJ. A Blank Slate? Layer-by-Layer Deposition of Hyaluronic Acid and Chitosan onto Various Surfaces. Biomacromolecules. 2006 May;7(5):1610–22.

60. Fu J, Ji J, Yuan W, Shen J. Construction of anti-adhesive and antibacterial multilayer films via layer-by-layer assembly of heparin and chitosan. Biomaterials. 2005 Nov;26(33):6684–92.

61. Girotti A, Reguera J, Arias FJ, Alonso M, Testera AM, Rodríguez-Cabello JC. Influence of the Molecular Weight on the Inverse Temperature Transition of a Model Genetically Engineered Elastin-like pH-Responsive Polymer. Macromolecules. 2004 May;37(9):3396–400.

62. McPherson DT, Morrow C, Minehan DS, Wu J, Hunter E, Urry DW. Production and purification of a recombinant elastomeric polypeptide, G-(VPGVG)19-VPGV, from Escherichia coli. Biotechnol. Prog. 1992 Aug;8(4):347–52.

63. Girotti A, Reguera J, Rodríguez-Cabello JC, Arias FJ, Alonso M, Matestera A. Design and bioproduction of a recombinant multi(bio)functional elastin-like protein polymer containing cell adhesion sequences for tissue engineering purposes. J Mater Sci Mater Med. 2004 Apr;15(4):479–84.

64. Drelich J, Mittal KL. Atomic force microscopy in adhesion studies. CRC Press; 2005.

65. Faulstich H, Zobeley S, Rinnerthaler G, Small JV. Fluorescent phallotoxins as probes for filamentous actin. Journal of muscle research and cell motility. 1988;9(5):370–83.

66. Kubista M, Aakerman B, Norden B. Characterization of interaction between DNA and 4', 6-diamidino-2-phenylindole by optical spectroscopy. Biochemistry. 1987;26(14):4545–53.

67. Zhu Y, Gao C, He T, Liu X, Shen J. Layer-by-Layer Assembly To Modify Poly(l-lactic acid) Surface toward Improving Its Cytocompatibility to Human Endothelial Cells. Biomacromolecules. 2003 Mar;4(2):446–52.

68. No HK, Prinyawiwatkul W. Stability of chitosan powder during long-term storage at room temperature. J. Agric. Food Chem. 2009 Sep 23;57(18):8434–8.

69. Boddohi S, Killingsworth CE, Kipper MJ. Polyelectrolyte Multilayer Assembly as a Function of pH and Ionic Strength Using the Polysaccharides Chitosan and Heparin. Biomacromolecules. 2008 Jul;9(7):2021–8.

70. Lawrie G, Keen I, Drew B, Chandler-Temple A, Rintoul L, Fredericks P, et al. Interactions between Alginate and Chitosan Biopolymers Characterized Using FTIR and XPS. Biomacromolecules. 2007 Aug;8(8):2533–41.

71. Kolhe P, Kannan RM. Improvement in ductility of chitosan through blending and copolymerization with PEG: FTIR investigation of molecular interactions. Biomacromolecules. 2003 Feb;4(1):173–80.

72. Wan Y, Wu H, Yu A, Wen D. Biodegradable Polylactide/Chitosan Blend Membranes. Biomacromolecules. 2006 Apr;7(4):1362–72.

73. Wan Y, Creber KAM, Peppley B, Bui VT. Structure and ionic conductivity of a series of di-o-butyrylchitosan membranes. Journal of Applied Polymer Science. 2004 Dec 15;94(6):2309–23.

74. Stoch A, Jastrzębski W, Brożek A, Stoch J, Szaraniec J, Trybalska B, et al. FTIR absorption–reflection study of biomimetic growth of phosphates on titanium implants. Journal of Molecular Structure. 2000;555(1):375–82.

75. Barrere F, Van Blitterswijk CA, De Groot K, Layrolle P. Influence of ionic strength and carbonate on the Ca-P coating formation from SBFx5 solution. Biomaterials. 2002;23(9):1921–30.

76. Barth A. Infrared spectroscopy of proteins. Biochimica et Biophysica Acta (BBA) - Bioenergetics. 2007 Sep;1767(9):1073–101.

77. De Souza NC, Zucolotto V, Silva JR, Santos FR, Dos Santos DS Jr, Balogh DT, et al. Morphology characterization of layer-by-layer films from PAH/MA-co-DR13: the role of film thickness. J Colloid Interface Sci. 2005 May 15;285(2):544–50.

78. Hu, Neoh KG, Cen L, Kang E-T. Cellular Response to Magnetic Nanoparticles “PEGylated” via Surface-Initiated Atom Transfer Radical Polymerization. Biomacromolecules. 2006 Mar;7(3):809–16.

79. Spoerke ED, Anthony SG, Stupp SI. Enzyme Directed Templating of Artificial Bone Mineral. Advanced Materials. 2009 Jan 26;21(4):425–30.

80. Liu Q, Ding J, Mante FK, Wunder SL, Baran GR. The role of surface functional groups in calcium phosphate nucleation on titanium foil: a self-assembled monolayer technique. Biomaterials. 2002;23(15):3103–11.

81. Liang F, Zhou L, Wang K. Apatite formation on porous titanium by alkali and heat-treatment. Surface and Coatings Technology. 2003;165(2):133–9.

82. Li F, Feng QL, Cui FZ, Li HD, Schubert H. A simple biomimetic method for calcium phosphate coating. Surface and Coatings Technology. 2002;154(1):88–93.

83. Barrére, Layrolle P, Van Blitterswijk CA, De Groot K. Biomimetic calcium phosphate coatings on Ti6AI4V: a crystal growth study of octacalcium phosphate and inhibition by Mg2 and HCO3-. Bone. 1999;25(2 Suppl):107S–111S.

84. Habibovic P, Barrere F, Blitterswijk CA, Groot K, Layrolle P. Biomimetic hydroxyapatite coating on metal implants. Journal of the American Ceramic Society. 2002;85(3):517–22.

85. Costantini A, Luciani G, Branda F, Ambrosio L, Mattogno G, Pandolfi L. Hydroxyapatite coating of titanium by biomimetic method. Journal of Materials Science: Materials in Medicine. 2002;13(9):891–4.

86. Arai Y, Sparks DL. ATR–FTIR Spectroscopic Investigation on Phosphate Adsorption Mechanisms at the Ferrihydrite–Water Interface. Journal of Colloid and Interface Science. 2001 Sep;241(2):317–26.

87. Teleb SM, Nassr DES, Nour EM. Synthesis and infrared spectra of alkaline earth metal carbonates formed by the reaction of metal salts with urea at high temperature. Bulletin of Materials Science. 2004;27(6):483–5.

88. Shah NJ, Hong J, Hyder MN, Hammond PT. Osteophilic Multilayer Coatings for Accelerated Bone Tissue Growth. Advanced Materials. 2012 Mar 15;24(11):1445–50.

89. Badami AS, Kreke MR, Thompson MS, Riffle JS, Goldstein AS. Effect of fiber diameter on spreading, proliferation, and differentiation of osteoblastic cells on electrospun poly (lactic acid) substrates. Biomaterials. 2006;27(4):596–606.

90. Deligianni DD, Katsala ND, Koutsoukos PG, Missirlis YF. Effect of surface roughness of hydroxyapatite on human bone marrow cell adhesion, proliferation, differentiation and detachment strength. Biomaterials. 2000;22(1):87–96.

91. Bronner F, Farach-Carson MC. Bone Formation (Topics in Bone Biology). 1st ed. Springer-Verlag; 2004.

92. Eijken M. Human Osteoblast Differentiation and Bone Formation: Growth Factors, Hormones and Regulatory Networks. 2007.

93. Fakhry A, Schneider GB, Zaharias R, Senel S. Chitosan supports the initial attachment and spreading of osteoblasts preferentially over fibroblasts. Biomaterials. 2004 May;25(11):2075–9.

94. Pieper JS, Van Wachem PB, Van Luyn MJA, Brouwer LA, Hafmans T, Veerkamp JH, et al. Attachment of glycosaminoglycans to collagenous matrices modulates the tissue response in rats. Biomaterials. 2000 Aug;21(16):1689–99.

95. Tierney CM, Jaasma MJ, O'Brien FJ. Osteoblast activity on collagen-GAG scaffolds is affected by collagen and GAG concentrations. Journal of Biomedical Materials Research Part A. 2009 Oct;91A(1):92–101.

96. Pieper JS, Oosterhof A, Dijkstra PJ, Veerkamp JH, Van Kuppevelt TH. Preparation and characterization of porous crosslinked collagenous matrices containing bioavailable chondroitin sulphate. Biomaterials. 1999 May;20(9):847–58.

97. Zhao C, Cao P, Ji W, Han P, Zhang J, Zhang F, et al. Hierarchical titanium surface textures affect osteoblastic functions. Journal of Biomedical Materials Research Part A. 2011 Dec 15;99A(4):666–75.

98. Engler AJ, Sen S, Sweeney HL, Discher DE. Matrix Elasticity Directs Stem Cell Lineage Specification. Cell. 2006 Aug;126(4):677–89.

99. Cheng M, Deng J, Yang F, Gong Y, Zhao N, Zhang X. Study on physical properties and nerve cell affinity of composite films from chitosan and gelatin solutions. Biomaterials. 2003 Aug;24(17):2871–80.

100. Yang YC, Chang E, Lee SY. Mechanical properties and Young's modulus of plasma-sprayed hydroxyapatite coating on Ti substrate in simulated body fluid. Journal of Biomedical Materials Research Part A. 2003;67A(3):886–99.

101. Grössner-Schreiber B, Griepentrog M, Haustein I, Müller WD, Lange KP, Briedigkeit H, et al. Plaque formation on surface modified dental implants. An in vitro study. Clin Oral Implants Res. 2001 Dec;12(6):543–51.

102. Lamont RJ, Gil S, Demuth DR, Malamud D, Rosan B. Molecules of Streptococcus gordonii that bind to Porphyromonas gingivalis. Microbiology. 1994;140(4):867–72.

103. Richert L, Boulmedais F, Lavalle P, Mutterer J, Ferreux E, Decher G, et al. Improvement of Stability and Cell Adhesion Properties of Polyelectrolyte Multilayer Films by Chemical Cross-Linking. Biomacromolecules. 2004 Mar 1;5(2):284–94.

104. Almaguer-Flores A, Ximénez-Fyvie LA, Rodil SE. Oral bacterial adhesion on amorphous carbon and titanium films: Effect of surface roughness and culture media. Journal of Biomedical Materials Research Part B: Applied Biomaterials. 2010;92B(1):196–204.